Soil CO_2 emissions at Furnas volcano (São Miguel Island, Azores archipelago) - volcano monitoring perspectives, geomorphologic studies and land-use planning application

Fátima Viveiros [(1)*]; Carlo Cardellini [(2)]; Teresa Ferreira [(1)]; Stefano Caliro [(3)]; Giovanni Chiodini [(3)]; Catarina Silva[(1)]

[(1)] Centro de Vulcanologia e Avaliação de Riscos Geológicos, Universidade dos Açores, Portugal. Maria.FB.Viveiros@azores.gov.pt

[(2)] Dipartimento di Scienze della Terra, Università di Perugia, Italy

[(3)] INGV- Sezione di Napoli, Osservatorio, Napoli, Italy

Abstract

Carbon dioxide (CO_2) diffuse degassing structures (DDS) at Furnas Volcano (São Miguel Island, Azores) are mostly associated with the main fumarolic fields, evidence that CO_2 soil degassing is the surface expression of rising steam from the hydrothermal system. Locations with anomalous CO_2 flux are mainly controlled by tectonic structures oriented WNW-ESE and NW-SE and by the geomorphology of the volcano, as evidenced by several DDS located in depressed areas associated with crater margins. Hydrothermal soil CO_2 emissions in Furnas volcano are estimated to be ~ 968 t d^{-1}. Discrimination between biogenic and hydrothermal CO_2 was determined using a

statistical approach and the carbon isotope composition of the CO_2 efflux. Different sampling densities were used to evaluate uncertainty in the estimation of the total CO_2 flux, and showed that a low density of points may not be adequate to quantify soil emanations from a relatively small DDS. Thermal energy release associated to diffuse degassing at Furnas caldera is about 118 MW (from an area of ~ 4.8 km^2) based on the H_2O/CO_2 ratio in fumarolic gas. The DDS affect also Furnas and Ribeira Quente villages, which are located inside the caldera and in the south flank of the volcano, respectively. At these sites, 58% and 98% of the houses are built over hydrothermal CO_2 emanations, and the populations are at risk due to potential high concentrations of CO_2 accumulating inside the dwellings.

Keywords: Soil diffuse degassing; soil CO_2 flux; emission rates; Azores archipelago

1. Introduction

Research performed in the last two decades has shown the importance of CO_2 contributions to the atmosphere from different quiescent volcanoes around the world [e.g. *Farrar et al.*, 1995; *Chiodini et al.,* 1998; 2004; *Gerlach et al.*, 1998; *Hernández et al.*, 1998; *Kerrick,* 1998; *Sorey et al.*, 1998; *Werner et al.*, 2000; *Brombach et al*., 2001; *Salazar et al*., 2001; *Lewicki et al*., 2003; *Werner and Brantley*, 2003; *Frondini et al*., 2004; *Padròn et al*., 2008; *Werner et al.*, 2008]. Determination of soil CO_2 concentrations and observation of spatial variations in flux provide important tools for identification of tectonic structures [*Toutain and Baubron*, 1999; *Baubron et al*., 2002; *Aiuppa et al*., 2004; *Chiodini et al*., 2004; *Carapezza et al*., 2009], for geothermal exploration [*Bergfeld et al*., 2001; *Fridriksson et al*., 2006; *Werner and Cardellini*, 2006; *Chiodini et al*., 2007; *Revil et al*., 2008] and for monitoring active volcanoes [*Giammanco et al*., 1998; *Bruno et al*., 2001; *Hernández et al*., 2001a, 2001b; *Caracausi et al*., 2003; *Carapezza et al*., 2004; *Notsu et al*., 2005; *Giammanco et al*., 2006; *Granieri et al*., 2006, *Chiodini et al*., 2001, 2008, 2009]. However, few studies have addressed the importance of diffuse CO_2 degassing in land-use planning to assess public health risks [*Baxter et al*., 1999; *Beaubien et al.*, 2003; *Annunziatellis et al*., 2003; *Barberi et al*., 2007].

In undertaking these types of studies, it has to be considered that several methodological factors influence soil CO_2 flux estimations, as for example the selection of the sampling methodology [*Carapezza and Granieri*, 2004], the survey strategy [*Cardellini et al.,* 2003] and the geostatistical approach [*Cardellini et al*., 2003; *Lewicki et al*., 2005]. In the last two decades several interpolation methods have been applied to produce maps of soil degassing. *Cardellini et al*. [2003] showed that sequential Gaussian simulations (sGs) are a reliable tool to model the spatial variability of soil diffuse degassing

processes, because it does not attenuate the extreme values and allows the estimation of the uncertainty. The sGs method is now widely used to study soil diffuse degassing processes in volcanic-hydrothermal environments [e.g. *Chiodini et al*., 2004; *Frondini et al*., 2004; *Caliro et al*., 2005; *Lewicki et al.*, 2005; *Fridrikson et al*., 2006; *Granieri et al*., 2006; *Werner and Cardellini*, 2006; *Chiodini et al*., 2007; *Padròn et al*., 2008; *Werner et al*., 2008].

Another critical point in the study of soil CO_2 degassing in volcanic-hydrothermal areas is the identification of CO_2 sources, such as biogenic and volcanic-hydrothermal derived CO_2. In locations with multiple diffuse emission sources, a statistical approach, e.g. graphical statistical analysis (GSA) [*Sinclair*, 1974; *Chiodini et al*., 1998] is commonly used to distinguish the amount contributed from each source. This approach provides a qualitative interpretation, however, if fluxes from multiple sources are of the same order of magnitude, then the method will not work. Recently, *Chiodini et al*. [2008] developed a new methodology based on the carbon isotopic composition of the soil CO_2 efflux that better constrain CO_2 origins.

In this work we apply soil CO_2 flux techniques in an Azorean volcano for the first time and calculate diffuse CO_2 emissions at Furnas volcano, comparing it with other hydrothermal-volcanic areas of the world. Based on anomalous CO_2 distributions, the main diffuse degassing structures (DDS) [*Chiodini et al*., 2001] for Furnas volcano are defined, which combined with morphological and geological observations supply useful information to understand the deep structures in the volcanic system. Different carbon sources are distinguished in Furnas volcano area, both through a statistical approach (GSA method) and $\delta^{13}C$ data interpretation.

At Furnas village (1541 inhabitants) CO_2 emanations are recognized as permanent and hidden threat [*Baxter et al*., 1999; *Viveiros et al.*, 2009], in addition to hazards from volcanic eruptions, seismic events [*Cole et al.*, 1995; *Silveira et al*., 2003] and landslides [*Valadão et al*., 2002].

Ribeira Quente village, in the S-SE flank of the volcano, has 798 residents [*Census*, 2001]. Given the risks for health, this work intends to be useful for volcano monitoring and also provides a valuable tool for land-use planning at Furnas volcano.

2. Geological setting and previous studies

The Azores archipelago is formed by nine volcanic islands located in the North Atlantic Ocean where the American, Eurasian and the African plates meet at a triple junction [*Searle*, 1980]. The main tectonic features are (1) the Mid-Atlantic Ridge (MAR) that crosses the archipelago between the islands of Flores and Faial; (2) the East Azores Fracture Zone (EAFZ), which extends E-W from the MAR to Gibraltar including the Gloria Fault and the (3) Terceira Rift (TR), which trends NW-SE from the MAR to the island of Santa Maria [e.g. *Machado,* 1959; *Searle*, 1980; *Madeira and Ribeiro*, 1990; *Vogt and Jung*, 2004] (Figure 1a).

São Miguel Island is the biggest island of the archipelago and comprises three trachytic polygenetic volcanoes (Sete Cidades, Fogo and Furnas) linked by rift zones (Figure 1b). Furnas volcano is located in the eastern part of the island and the first rocks are dated from about 100,000 years BP [*Moore*, 1990]. Morphologically, Furnas comprises an impressive 5 x 8 km summit depression formed by two nested calderas controlled by NW-SE and NE-SW faults [*Guest et al*., 1999]. The younger caldera contains several craters and the western part is dominated by a lake that occupies an area with 1.9 km^2 [*Cruz et al*., 2006]. Most of the inhabited part of Furnas village is located in the bottom of Furnas "c" crater [*Guest et al*., 1999] (Figure 1c).

Activity at Furnas volcano is characterized by several eruptive styles ranging from effusive to caldera-forming explosive events [*Guest et al*., 1999]. Since the settlement of the island in the 15th Century, two intracaldera volcanic eruptions occurred at Furnas volcano in 1439-43 [*Queiroz et al*., 1995] and in 1630 [*Booth et al*., 1978; *Cole et al*., 1995] with the formation of two tuff rings with central domes that occupy part of the

caldera floor. The 1630 subplinian eruptive event was responsible for the death of about 200 persons, mostly at the Ponta Garça village, SW of the volcano [*Cole et al*., 1995].

One of the most important fracture systems at Furnas volcano crosses the volcanic edifice along a WNW-ESE trend and shows a clear normal dip-slip component (Figure 1c). Conjugate faults with N-S and (N)NE-(S)SW trends and extensional fractures with NW-SE direction parallel to the Terceira Rift regional fault system are also observed [*Gaspar et al*., 1995; *Guest et al*., 1999; *Carmo*, 2004].

At present, secondary manifestations of volcanism are characterized by boiling temperature fumaroles (95 to 100ºC), steaming ground, thermal springs, cold CO_2-rich springs (Figure 1c) and diffuse CO_2 degassing areas [*Ferreira et al.*, 2005]. Most of the hydrothermal manifestations are located inside the caldera and include three main fumarolic fields (Figure 1c). Several areas of steaming ground are present on the S flank of the volcano, at Ribeira Quente village. Fumarole gas is mostly comprised of water (steam) and CO_2. H_2S, H_2, N_2, O_2, CH_4 and Ar are present in lower concentrations [*Ferreira and Oskarsson*, 1999; *Ferreira et al*., 2005]. Previous studies [*Cruz et al*., 1999; *Ferreira and Oskarsson*, 1999] proposed that the fumarolic discharge at Furnas volcano is sustained by steam separation from aquifers at 100-200 m depth with a maximum temperature of 180ºC and are supplied with gas from plutonic bodies cooling at greater depths.

In the early nineties the first diffuse degassing studies were performed in the Azores archipelago, exactly at Furnas volcano [*Baubron et al*., 1994]. Soil CO_2 concentration measurements in the inhabited area of the caldera, essentially inside Furnas "c" crater, oscillated from 0 to 100 vol.% at 70 cm (Figure 2a). Based on this work, *Baxter et al.* [1999] estimated that about one-third of the houses at Furnas village were placed over

an important soil diffuse degassing area. *Sousa* [2003] repeated the soil CO_2 concentration measurements and found that even if the density of points was different, the location of the main anomalous soil CO_2 areas was similar to the earlier survey (Figure 2b).

Two permanent soil CO_2 flux stations and meteorological sensors were established at Furnas volcano in 2001. The acquired data on those stations show that meteorological variables have significant control on the gas flux fluctuations [*Viveiros et al*., 2008].

3. Material and methods

Soil CO_2 flux surveys were performed at Furnas volcano mostly during the summer months of 2005 and 2007. Sporadic measurements were carried out in 2006 and 2008 to better delineate some gas anomalies.

Soil CO_2 fluxes were measured in 2605 points at Furnas volcano. A general survey consisted in 1756 measurements (Figure 3a, data set A1 in Table 1) including 1362 randomly distributed at distances between 50 – 100 m, depending on the accessibility of the sites, and 394 measurements were performed along profiles. The set of 1362 randomly distribute measurements (data set A2 in Table 1) covers the intracaldera area (~ 5.8 km^2), including the three main fumarolic fields, from Furnas lake, on the W side of the caldera, to Ribeira dos Tambores, in the E side, and the area of Furnas village. The surveyed area is characterized by the presence of different types of vegetation such as, grassland, cultivated lands and forest. Measurements in forested areas were avoided, when possible.

Detailed surveys were performed at Furnas lake fumarolic area (data set B in Table 1), Furnas village fumarolic area (data set C in Table 1) and Ribeira Quente village (data set D in Table 1). The Ribeira Quente village was surveyed for the first time, with the main objective to evaluate the gas hazard connected to soil degassing and this survey consisted in 148 measurements performed on an irregular grid covering an area of 0.35 km^2. The spatial distribution of measurements was strongly influenced by geomorphologic features and by the presence of anthropogenic infrastructures (e.g., houses and roads). In the villages area (Furnas and Ribeira Quente) the measurement spacing was reduced to about 10-15 m.

Furnas lake and Furnas village fumaroles surveys were performed in order to better define the degassing pattern in the vicinities of the main fumarolic fields. The two areas were investigated with a great detail using a sampling spacing between 3–7 m (Figures 3b and 3c).

In addition, 88 soil CO_2 flux measurements were performed outside Furnas volcano (data set E in Table 1) in two basaltic rift zones with no hydrothermal manifestations (Achada das Furnas Plateau and Picos Waist Zone) (Figure 1b) and type of vegetation similar to that of Furnas volcano (i.e., grass, scrub, trees, etc.).

Soil CO_2 flux measurements were performed using portable instruments (manufactured by West Systems S.r.l.) based on the accumulation chamber method [*Norman et al*., 1992; *Chiodini et al*., 1998]. The two instruments were equipped, one with a LICOR LI-800 infrared CO_2 detector (L-IR) and the other with a Dräger Polytron infrared CO_2 detector (D-IR).

The L-IR measures CO_2 concentrations in the range from 0 to 2 vol.%. The reproducibility was estimated around 10% for CO_2 fluxes between 10 to 10000 g $m^{-2}d^{-1}$ by *Chiodini et al*. [1998], using a similar instrument. *Carapezza and Granieri* [2004] found that the uncertainty increased to 24% for measurements in low soil CO_2 flux areas. D-IR measures CO_2 concentrations in the range from 0 to 100 vol.%, and allows more accurate measurements for higher soil CO_2 fluxes.

In order to compare the performance of the two instruments, equipped with the two detectors, CO_2 fluxes were measured at different sites using both instruments. In areas with low and high soil CO_2 flux values, the D-IR full scale was set to 2 and 100 vol.%, respectively. The measured CO_2 fluxes varied less than 10% between the two instruments until soil CO_2 flux values lower than 10000 g m^{-2} d^{-1}. At higher CO_2 fluxes

(between 10000 and 25000 g m^{-2} d^{-1}) the L-IR equipped instrument produced flux measurements higher than the D-IR equipped instrument. This discrepancy can occur because, for such high fluxes, the full scale of the L-IR is suddenly reached and the increment of CO_2 concentration in the time (i.e., CO_2 flux) can not be accurately determined. On contrary, at the same conditions, the increase of the CO_2 is well measured when the D-IR is used.

The detailed surveys at Furnas lake and Furnas village fumaroles (data sets B and C, Table 1) were performed using the CO_2 flux portable instrument equipped with D-IR. The general survey (data sets A1 and A2, Table 1) and the Ribeira Quente village survey (data set D, Table 1) were performed entirely using the CO_2 flux portable instrument equipped with L-IR, because D-IR was not available at that time. Fourteen of the CO_2 fluxes measured with L-IR that exceeded the maximum measurable flux given by the equipment manufacturing company (25000 g m^{-2} d^{-1}), were assigned a value of 25000 g m^{-2} d^{-1}. For this reason, the true maximum CO_2 flux for the area may have not been measured.

Due to the influence of the meteorological parameters on the soil gas flux [e.g. *Chiodini et al.*, 1998*; Granieri et al*., 2003; *Viveiros et al*., 2008, 2009], the surveys were carried out during dry days with similar and stable weather conditions. Data acquired by the permanent soil CO_2 flux station at Furnas lake (GFUR2) (Figure 3a) were used to check meteorological variations. In addition, data acquired at the permanent flux station and at some other selected points showed a coefficient of variation for the soil CO_2 flux around 12% during the surveyed periods, a value considered acceptable taking into consideration that the reproducibility of the used instrument is about 10%.

Gas samples for the determination of the carbon isotope composition of the CO_2 efflux were collected at twelve points (Figure 3a), with a range of soil CO_2 flux and vegetation type. The gas was collected in pre-evacuated bottles simultaneously with the soil CO_2 flux measurement following the procedures described by *Chiodini et al*. [2008]. One sample was collected in the high soil CO_2 flux areas and the air CO_2 inside the bottle was higher than 2 vol.%. For low soil CO_2 flux measurement points, two samples were collected; one sample was collected just after the homogenization of the gases within the accumulation chamber and the second bottle was sampled at higher CO_2 concentrations (always higher than 1000 ppm) (Table 2). Soil temperature was measured at each site using a thermocouple at 20 cm depth.

Gas samples were analyzed for chemical and isotopic composition at the Laboratory of Fluids Geochemistry of INGV-Osservatorio Vesuviano. CO_2 concentrations and carbon isotope compositions were determined by coupling a gas chromatograph (Agilent Technologies 6890N, GC) with a continuous flow mass spectrometer (Finnigan Delta plusXP, MS) ($\delta^{13}C$ standard error ± 0.1‰, CO_2 concentration standard error ± 3%). The GC is equipped with a capillary column (HP-plotQ capillary, 30m x 0.53mm x 25μm; He as carrier gas), TCD detector and a post column switching device, able to switch or split the column gas flow to the TCD detector and to the MS. During the analysis air components are completely switched to the GC detector (TCD), preventing the formation of undesirable species in the MS source (NO_x).

The CO_2 flux values were elaborated using both the graphical statistical analysis method (GSA) described by *Chiodini et al*., [1998] and sequential Gaussian simulations (sGs) [*Cardellini et al*., 2003]. The GSA method consists of partitioning complex statistical data distribution, which results from overlapping log normal populations, into

individual populations. The mean, the standard deviation and the proportion of each partitioned log normal population are graphically estimated by applying the procedure proposed by *Sinclair* [1974]. Since statistical parameters refer to the logarithm of the values, the mean CO_2 flux and the 90% confidence interval of the mean are then computed with the Sichel t-estimator [*David*, 1977].

The sGs method is used to produce a map of the CO_2 flux and therefore to define the shape and the extension of the DDS, as described by *Cardellini et al*. [2003]. The sGs method consists of the production of numerous simulations of the spatial distribution of the attribute (flux), and is performed using the algorithm described by *Deutsch and Journel* [1998].

Since the sGs procedure requires a multi-Gaussian distribution, original data were transformed into normal distribution by a normal score transform [*Deutsch and Journel*, 1998; *Cardellini et al*., 2003]. Experimental variograms were computed and modeled for each data set. The models were used in the sGs procedure to create 100 realizations of the flux grid.

For the visualization of the simulation results, we used both probability and E-type maps. The probability map reports the probability that the simulated value at each location is higher than a selected threshold and is used to better identify the DDS. The E-type map shows the "expected" value at any location (E-type estimate), obtained through a point-wise linear average of all the simulations.

The CO_2 released by diffuse degassing was calculated for the different data sets by integrating the average values estimated from sGs (i.e., E-Type map) over the area. The mean and the standard variation computed for the 100 realizations are, thus, assumed to be the characteristic values of the CO_2 release and of its uncertainty for each area.

Diversity across the different groups was evaluated using coefficient of variation (CV), a statistical index calculated as the ratio of the standard deviation to the average and usually reported as a percentage [*Reed et al*., 2002].

4. Results and discussion

4.1 Hydrothermal and Biogenic soil CO_2 fluxes

At Furnas volcano soil CO_2 flux values were highly variable, ranging from 0 to values higher than 25000 g m^{-2} d^{-1} (Table 1) and all data sets are positively skewed. Excluding all values above 10000 g m^{-2} d^{-1}, which should be mainly related to viscous flux measured on steam vents, the remaining soil CO_2 flux values from Furnas volcano (data set referred as A1, Table1) were modeled applying the procedure proposed by *Sinclair* [1974], as combination of three overlapping log-normal populations (Figure 4). This polymodal distribution suggests the existence of multiple sources (biogenic and volcanic-hydrothermal) feed overall soil CO_2 diffuse degassing. The estimated mean, 90% confidence interval of the mean and the proportion of partitioned populations are reported in Table 3.

Population "Aa" (Table 3), representing only 2% of the data, is characterized by very low soil CO_2 flux values (mean CO_2 flux ~ 2.3 g m^{-2} d^{-1}). These very low CO_2 fluxes occur in poorly vegetated areas, i.e., where the biologic production of CO_2 is scarce, or from areas where the soil is highly altered being impermeable and compacted.

Population "Ac" (22% of the data) is characterized by a mean CO_2 flux of ~ 500 g m^{-2} d^{-1}, and can be considered representative of CO_2 fluxes fed by an endogenous source, i.e., by the degassing of the hydrothermal system [e.g., *Chiodini et al*., 1998, 2001, 2007, 2008; *Cardellini et al*., 2003].

The most abundant population, "Ab", including ~ 76% of the data, is characterized by a mean CO_2 flux significantly lower (~ 32 g m^{-2} d^{-1}) than population "Ac". If we assume that population "Ab" is representative of the biological CO_2 flux, choosing the 95th percentile of population "Ab" as cutoff (Figure 4) for the biological (background) CO_2

fluxes, this results in a flux of 80 g m^{-2} d^{-1}, too high for a purely biogenic CO_2 flux. In fact, available data on CO_2 production from a wide variety of ecosystems show CO_2 fluxes ranging from 0.2 to 21 g m^{-2} d^{-1} [e.g., *Raich and Schlesinger*; 1992; *Raich and Tufekcioglu*, 2000] with maximum flux values for grassland as ~ 50 g m^{-2} d^{-1} [e.g., *Norman et al*., 1992; *Bajracharya and Kimble*, 2000; *Nakadai et al*., 2002]. In addition, the soil CO_2 fluxes measurements performed outside Furnas volcano (data set E in Table 1) in areas with vegetation types similar to that of the studied area (i.e., grass, scrub, trees, etc.), did not exceed 34 g m^{-2} d^{-1}. More in detail, the CO_2 fluxes performed outside Furnas volcano show two distinct populations, one (34% of samples) characterized by a mean CO_2 flux of 1 g m^{-2} d^{-1} (standard deviation = 0.36), the other (66% of samples), characterized by a mean CO_2 flux of 22 g m^{-2} $d^{-}1$ (standard deviation = 5.54) (Figure 4).

As such, possible contributions to population "Ab" from a hydrothermal source must be considered.

In order to better understand the CO_2 flux populations distribution and to better constrain a reasonable threshold for the biogenic CO_2 background, the isotopic composition of the CO_2 efflux ($\delta^{13}C_{CO2}$) was investigated according with the method proposed by *Chiodini et al*., [2008]. The $\delta^{13}C_{CO2}$ values varied from -12.28 ‰ to -3.11 ‰, confirming that CO_2 from the hydrothermal system and from soil biological activity feed the diffuse CO_2 degassing (Table 2).

The isotopic composition of CO_2 of Caldeira Grande fumarole, measured in this study, ($\delta^{13}C$ = -4.26 ‰) is assumed as representative of the hydrothermal source of CO_2. This value agrees with the isotopic compositions of CO_2 from the main fumaroles located inside Furnas volcano caldera ($\delta^{13}C$ mean value of -4.05 ‰) [*Ferreira and Oskarsson*,

1999] and with the isotopic signature of the deep source of the carbon dissolved in CO_2-rich ground-waters of the area (~ -4 ‰) [*Cruz et al*., 1999].

It is more difficult to establish the isotopic composition of biogenically-produced CO_2, because C3 and C4 plants present at Furnas [Pereira, M.J., *personal communication*, 2009] produce CO_2 characterized by a large range in the isotopic composition (means $\delta^{13}C$ of about -27‰ and – 13‰ for C3 and C4 plants, respectively) [*Cheng*, 1996].

Following the approach performed by *Chiodini et al*. [2008] to model the soil CO_2 degassing at Solfatara volcano (Italy), measured $\delta^{13}C_{CO2}$ values and CO_2 flux values are compared in Figure 5 with the theoretical values expected for the mixing between biogenic and hydrothermal CO_2 sources. For a first test, two extreme cases were considered: (1) mixing between hydrothermally-derived CO_2 ($\delta^{13}C$ = -4.2 ‰) and a light biogenic CO_2 ($\delta^{13}C$ = -27‰) with a high efflux rate (50 g m^{-2} d^{-1}) and (2) mixing between hydrothermal CO_2 ($\delta^{13}C$ = -4.2 ‰) and a C4-derived biogenic CO_2 ($\delta^{13}C$ = -13‰) with a low CO_2 efflux rate (10 g m^{-2} d^{-1}). All the measured $\delta^{13}C_{CO2}$ data fall in the field delimited by the mixtures between hydrothermal CO_2 and the two extremes for biogenic CO_2, suggesting that the two cases can model all the soil CO_2 degassing at Furnas volcano.

Excluding one sample, a model considering the mixing of hydrothermal CO_2 and a biogenic source characterized by a $\delta^{13}C$ = -27‰ and an efflux rate of 25 g m^{-2} d^{-1}, seems to constrain the maximum magnitude of the biogenic flux (Figure 5). In other words, even with the low amount of isotopic data, a CO_2 efflux rate for the biological background should be between 10 and 25 g m^{-2} d^{-1} (~ 42% of the data), which is also in agreement with soil CO_2 flux measurements performed outside Furnas volcano area.

These results point out that population "Ab" (Table 3) is likely a mixture between biogenic and hydrothermal CO_2 fluxes and that the threshold value for the biogenic CO_2 flux of ~ 80 g m^{-2} d^{-1}, derived by assuming the "Ab" population as representative of the biogenic flux, constitutes an overestimation of the real one.

A similar overestimation of the biogenic background flux produced by the only interpretation of the probability plots of CO_2 fluxes was pointed out in the work of *Chiodini et al*. [2008], suggesting that the new methodology proposed by those authors, based on the isotopic composition of CO_2 efflux, is a powerful tool to better constrain all the CO_2 sources feeding soil CO_2 degassing.

4.2 Mapping and quantification of soil CO_2 degassing

Omnidirectional variograms of normal scores were computed (Figure 6). Experimental variograms for Furnas caldera data set and Ribeira Quente village data show nested structures (spherical and exponential) with different ranges and nugget values (Figures 6a and 6d). Data from Furnas lake and Furnas village fumaroles (data sets B and C, Table 1) have the highest nugget values (Figures 6b and 6c). The higher density of points and the higher nugget effects observed in the detailed surveys, carried out close to the Furnas lake and Furnas village fumarolic fields, contrast with the lower nugget effect observed in the variogram of the data collected in the Furnas caldera (data set A2, Table 1), where the points were sampled at a greater distance. This is probably explained by the heterogeneities in the soils properties near the fumaroles, where the soil alteration causes large differences in the permeability at very small scale.

One hundred equiprobable simulations were performed for each data set to estimate the soil CO_2 flux, and to evaluate the uncertainty of the estimation (Table 4). The CO_2 flux

data collected along transects performed across Furnas volcano were not used in the sGs simulation and are reported in the flux map of Figure 7 as single points with graded colors.

Probability maps derived from sGs results are used to better identify the DDS. As described earlier, on the basis of CO_2 flux measurements performed outside Furnas volcano and of the isotopic compositions of the CO_2 efflux, a reasonable mean value for the biogenic soil CO_2 flux could be considered about 25 g m^{-2} d^{-1}. For this reason, a value of 50 g m^{-2} d^{-1} (i.e., two times higher) was assumed as threshold in the probability map (Figure 8), to define the areas where the CO_2 flux is fed also by the hydrothermal source (i.e. the DDS). This choice of the threshold is somehow arbitrary, but could account for the variability of the biological CO_2 flux. The DDS are practically defined as those locations with a greater than 50% probability that the simulated CO_2 fluxes are at or above the threshold value.

The maps of Figures 7 and 8 show that high flux areas are found close to the main fumarolic fields (DDS labeled A, B and C) suggesting that in those areas CO_2 travels mostly with rising hydrothermal steam. The DDS B (Figure 7) is close to the Furnas village fumaroles and extends with a general NW-SE direction along the "Furnas c" northern crater limit. Soil CO_2 flux anomalies are observed also in the northern part of the younger caldera rim (DDS D, Figure 7) and "spots" of high soil CO_2 flux are dispersed in the bottom of Furnas "c" crater. On the eastern sector and in the south flank of the volcano, the high CO_2 flux values (> 100 g m^{-2} d^{-1}) are also found mainly associated to tectonic structures, with general WNW-ESE orientation. It is worth to note that the Ribeira Quente village, located in the south flank of the volcano, is characterized by soil CO_2 fluxes mostly higher than 50 g m^{-2} d^{-1} (i.e., it is built on a DDS).

4.2.1 Soil CO_2 flux and volcano/tectonic structures

By the inspection of the spatial distribution of soil CO_2 fluxes (Figures 7 and 8) emerges that three important anomalous zones of Furnas volcano (DDS A, B1, B2, D) are associated to craters (i.e., are located in the inner slope of craters rims, Figures 7 and 8a). This correspondence may suggest a main role of crater morphology on the CO_2 degassing process. Similar morphologic control was observed at Vesuvius volcano where CO_2 anomalies are mainly concentrated in the inner slopes of the crater [*Frondini et al*., 2004].

Despite this partial correspondence between DDS and craters, since i) anomalies are not observed in the inner slope of whole craters, ii) the general WNW-ESE trend in the DDS (e.g., alignment 1' and area E in Figure 8a) is coincident with the direction of the main faults mapped on the flanks of Furnas volcano [*Gaspar et al*., 1995; *Guest et al*., 1999], iii) similar directional pattern were described for anomalous CO_2 concentrations in soil gases in the previous work of *Sousa* [2003] (Figure 2b), it follows that the orientation of the DDS, including those associate to the craters, are primarily controlled by WNW-ESE oriented tectonic structures. For instance, the part of DDS B which extends outside Furnas "c" crater (DDS B2 in Figure 8a) is probably related to a tectonic structure extending from DDS D to DDS C. Most of these tectonic structures were not mapped previously, possibly because they are hidden by the presence of luxuriant vegetation and by thick pumice deposits of the caldera.

Diffuse degassing patterns observed in this work (Figures 7 and 8) do not display evidence of the W-E tectonic lineaments crossing Furnas caldera, as suggested by

previous studies [*Cruz et al*., 1999; *Ferreira and Oskarsson*, 1999] as the main structures controlling hydrothermal manifestations of the caldera floor.

Flux measurements in the central part of the Furnas caldera along profile P1-P1' (Figure 3), which crosses historical domes and tuff rings, show that these areas are characterized by low soil CO_2 flux values (Figure 9), essentially associated with the biogenic CO_2 source. These data suggest that, in general, dome-structures do not enhance degassing of CO_2 and that the domes can be considered completely degassed. The only evidence of hydrothermal CO_2 degassing is associated with the 1630 eruption deposits at the intersection of the dome with the surface. This is probably due to some residual gas that is conducted along contact of the dome with the surroundings (Figures 7 and 9).

The measurements performed in the eastern area of the caldera, in the western part of the lake and in the south flank of the volcano show several anomalous "spots" probably related with the tectonic structures that cut the volcano flanks. In fact, these soil CO_2 flux measurements confirm the presence of some previously inferred faults.

Relatively to Ribeira Quente village area, anomalous diffuse degassing (DDS G, Figure 8b), as well as areas of steam emission, are located in western area of the village that was interested by an important landslide associated to the 1630 volcanic eruption. The DDS F (Figure 8b) is associated to the scarp of a landslide that occurred in 1997 caused by intense rainfall [*Marques et al*., 2007]. Another area of anomalous degassing is located in the western area of the village where the cliff is intersected by a NE-SW tectonic structure, suggesting also in this case a relation between tectonic structure and diffuse degassing.

Even if more structural data is necessary to complement, and fully understand, the degassing patterns, a strong structural control on the CO_2 degassing structures is

evident, confirming that mapping soil CO_2 degassing can constitute a useful tool to identify/verify the presence of hidden faults, which constitute weak zones that allows the rising up of deeply derived CO_2, as previously pointed out by several authors [e.g. *Chiodini et al.*, 2001; *Werner and Cardellini*, 2006]. This study can hence constitute a useful support for future structural studies at the Furnas caldera.

4.2.2 CO_2 emissions to the atmosphere

On the basis of sGs results a mean CO_2 release of 959 t d^{-1} (± 84 t d^{-1}) was estimated at Furnas caldera (area of 5.8 km^2). The computed CO_2 release varies from ~ 745 t d^{-1} to ~ 1227 t d^{-1} among the 100 realizations (Table 4). The estimated CO_2 release has a relatively low uncertainty and a CV of 9 % (Table 4).

Even if the CO_2 emissions estimate for Furnas Caldera has a low uncertainty, in order to verify and improve the accuracy of the estimate, the CO_2 release computed for the Furnas lake and Furnas village fumaroles areas, using only the data from Furnas caldera survey (Refs. A2.1 and A2.2 in Table 4; Figures 10b and d), was compared with the CO_2 release estimates obtained from the detailed surveys performed in the same areas (Refs B and C in Table 4; Figures 10a and c).

It is possible to observe that CO_2 emissions estimated from the detailed surveys are about three times lower than those resulting from the Furnas caldera survey (Table 4). Nevertheless, even if the CO_2 emission was significantly different, the diffuse degassing pattern is still similar in the corresponding maps of Figure 10.

The differences observed in the CO_2 emission estimates can arise by the adequacy of the measuring grid used in the Furnas caldera general survey (e.g., sample density,

Table 4) for areas characterized by a strong spatial variability of CO_2 degassing. The high heterogeneity of the soils near the fumarolic grounds, which are covered by altered and impermeable deposits prevent the gas to pass homogeneously through all the soil and concentrate the gas emissions on the fumaroles and/or in areas with small cracks, justifying the variability of CO_2 degassing. These small scale heterogeneities were also evidenced by the higher nugget effect of the variogram models of the detailed surveys data (Figures 6b and c) respect to those of the caldera general survey (Figures 6a and d). The density of points used in this work to produce the Furnas caldera CO_2 emissions maps (Figures 7 and 8a), 233 points/km^2, is comparable to other degassing surveys performed at other volcanoes (Table 5). In fact, for areas bigger than 3 km^2, a lower density of measuring points was generally adopted. With respect to our detailed surveys close the fumarolic fields, the number of points per 1 km^2 is higher than 8000 and shows much greater detail than found in any work reported in literature (Table 5).

Cardellini et al. [2003] suggested that the uncertainty in the estimation of the total CO_2 release is not simply correlated to the sample density but depends on the relation between the sample density and the extent of degassing structures. In particular, a general relation was derived by those authors, considering the number of samples falling in the area contained by a circle with radius equal to the range of the CO_2 flux variogram (circle range area (CRA)). We used the empirical relation derived by *Cardellini et al.* [2003]:

$$E.sd = 119.9 \times ns_{CRA}^{-0.55} \quad (1)$$

where $E.sd$ is the estimated standard deviation (%) of the CO_2 total release estimation and ns_{CRA} is the number of samples in CRA, to evaluate the expected standard deviation of the CO_2 flux estimates for the different dataset.

The *E.sd* for Furnas lake and Furnas village fumaroles detailed surveys results 7% and 3% of the total CO_2 output, considering the respective surveyed areas, number of samples (Table 1) and range of the variograms (i.e., 80 and 150 m, respectively, Figure 6), These low *E.sd* point out the adequacy of the sampling design used in the detailed surveys of the two sites.

The *E.sd* computed for Furnas caldera survey (i.e., range of the variogram = 300 m, Figure 6a), gives an uncertainty of about 12%, suggesting the adequacy of the number of sampling points to describe the entire study area. However if we consider the Furnas caldera sampling design and an anomaly with an average range of 115 m as representative of the DDS at Furnas lake and Furnas village fumaroles, we obtain from Equation 1 an *E.sd* of 34%. This higher *E.sd* points out that the sampling pattern adopted in the general survey of Furnas caldera (i.e., 50 – 100 m of sampling spacing) could not be adequate to quantify accurately CO_2 flux from the relatively small DDS, such as those characterizing the soil degassing at Furnas lake and Furnas village fumaroles.

Considering that the CO_2 output release of the Furnas lake and Furnas village fumarolic fields (obtained from the detailed surveys) is lower than that obtained for the same areas from the Furnas caldera survey (Table 4), the total CO_2 emission estimated at Furnas caldera (i.e., 959 t d^{-1}± 84 t d^{-1}) may represent an overestimation.

Taking in to account these results, a more accurate estimation of the CO_2 release from Furnas caldera is obtained considering for the Furnas lake and Furnas village fumaroles areas the CO_2 release estimated from the detailed surveys data (Refs. B and C, Table 4), instead of the CO_2 release estimated for the same areas from the Furnas caldera survey data (Refs. A2.1 and A2.2, Table 4). Following this approach the total CO_2 release from

Furnas volcano is estimated in ~ 880 t d^{-1}. This value includes both the hydrothermal and biogenic produced CO_2. The hydrothermal CO_2 emission is then computed in 734 t d^{-1} by subtracting to the estimated total CO_2 release the contribution from biogenic CO_2 flux. This contribution was estimated in 146 t d^{-1}, assuming that a mean biogenic CO_2 flux of 25 g m^{-2} d^{-1} is constant over all the area (excluding the steaming ground). This last assumption is an approximation, but considering that the extension of areas without vegetation is small with respect to the entire surveyed area, and that CO_2 fluxes up to 5000 g m^{-2} d^{-1} were measured in vegetated areas, it is reasonable to consider a biogenic CO_2 flux contribution also in the high degassing areas.

For the Ribeira Quente village area CO_2 release was estimated in ~ 243 t d^{-1} (± 43 t d^{-1}), and assuming also in this case a constant background, results that about 96% (~ 234 t d^{-1}) is from hydrothermal origin.

Hydrothermal CO_2 output from the whole Furnas volcano can thus be obtained by summing the estimations for Furnas caldera and Ribeira Quente village, resulting in a value of ~ 968 t d^{-1} (from an area with ~ 5.2 km^2).

Our estimate of hydrothermal CO_2 released by diffuse degassing at Furnas volcano is likely a minimum value, given that several soil CO_2 flux anomalous values were measured along the transects (Figure 7) and are not included in the estimations. In fact, due to difficult terrain, the extension of the gas anomalies along the road that links Ribeira Quente village to Ribeira dos Tambores and along the walking trail in the south flank of the volcano was not mapped. In addition, our estimates represent only the diffuse component of the CO_2 flux and do not account for contributions from fumaroles, bubbling pools or Furnas lake. As such, the total CO_2 emission from Furnas volcano is probably larger than our estimate.

Our estimates of CO_2 release are comparable to other important CO_2 degassing volcanic hydrothermal systems of the world (Table 5), pointing out the relevance of the diffuse degassing process at Furnas. Furthermore, if we consider the CO_2 emissions standardized per area (Tables 4 and 5), Furnas volcano is one of the larger CO_2 producing volcanoes. In fact, Furnas caldera CO_2 emission per area is similar to the summit of Miyakejima volcano (Table 5). Furthermore the soil CO_2 flux emitted close to the Furnas main fumarolic fields (data sets B and C, Table 4) are the same order of magnitude for Hot Spring Basin and Mud volcano areas in Yellowstone volcano [*Werner et al*., 2000, 2008].

The magnitude of diffuse CO_2 degassing at Furnas is relevant also if compared with the annual industrial CO_2 emission allocated by the European Commission for Portugal (EU press release IP/07/1566: "Emissions trading: Commission adopts decision on Portugal's national allocation plan for 2008-2012"). In fact the CO_2 naturally emitted by Furnas volcano results about 1% of the anthropogenic CO_2 production. This comparison, together with estimates at global scale of volcanic and non-volcanic natural CO_2 emissions [e.g. *Kerrick*, 2001; *Morner and Etiope*, 2002], contributes to reinforce the importance of the quantification of natural CO_2 diffuse fluxes for a refined global C-budget modeling.

5. Thermal energy release

The existence of CO_2 flux anomalies close to the fumarolic fields, and consequently associated to high temperature areas, suggest that the upflow of fluids from the underlying boiling hydrothermal reservoir and the steam condensation in the subsurface are responsible for the CO_2 diffuse degassing areas and the anomalous thermal gradients found at Furnas volcano. This process was simulated using a geothermal simulator (TOUGH2, Pruess, 1991) by *Chiodini et al*., [2005]. The results of the physical-numerical simulations showed that injection of fumarolic fluid into the soil produce a convective plume of hot carbon dioxide-steam mixture extending from the source toward the surface. During the ascent the upflowing steam condenses and produces a liquid phase that flows from the border of the plume toward the bottom of the simulated domain, whereas CO_2, which is non-condensable gas, is discharged almost entirely at the soil surface, feeding the CO_2 diffuse degassing. The heat released by diffuse degassing processes can be thus estimated by (1) measuring the total CO_2 output, (2) considering the chemical composition of fumaroles of the area as representative of the composition of the fluids before the steam condensation, and (3) computing the total steam output and the heat released during the condensation process and cooling of the condensates to ambient temperature [*Chiodini et al*., 2005].

In order to estimate the heat flux involved in the diffuse degassing processes at Furnas, it was assumed that the CO_2 is derived from hydrothermal fluid having the composition of the Caldeira Grande fumarole (from Furnas village fumarolic field), which was recognized as the only fumarole at Furnas caldera where uncontaminated hydrothermal fluid is discharged [*Ferreira and Oskarsson*, 1999]. The average H_2O/CO_2 ratio of 5.3 by weight of gas collected at the Caldeira Grande fumarole was thus considered as representative of the hydrothermal fluid before steam condensation. Consequently, a

value of 84.8 t d^{-1} of condensed steam is estimated to produce the 16 t d^{-1} of hydrothermal CO_2 released by diffuse degassing at Furnas village fumarolic field (Table 4). The energy released by the diffuse degassing process in this area has been estimated at ~ 2.6 MW, considering the total amount of condensed water and enthalpy of steam condensation at 100 ºC (2257 J g^{-1}, *Keenan et al*., 1969) and the cooling of condensate to 15 °C (i.e., mean ambient temperature). Appling the same approach to the diffuse degassing area at Furnas lake (~ 0.043 km^2), the thermal energy released in the area is estimated at ~ 2.1 MW.

A rough estimation for the thermal energy released inside Furnas caldera can be performed following the same methodology, even if the CO_2/H_2O ratio may suffer some variations in the caldera. Considering that the estimates for the hydrothermal CO_2 emission inside Furnas caldera is 734 t d^{-1} (from an area of ~ 4.8 km^2), a thermal energy released of ~ 118 MW was estimated.

The thermal energy released per km^2 at Furnas volcano degassing areas gives value similar to other quiescent volcanoes reported by *Chiodini et al*. [2005], and it is in the same order of magnitude as for example Nisyros DDS structures (Greece), Vesuvio cone (Italy), Vulcano crater (Italy) and Favara Grande fumarolic field (Pantelleria Island, Italy). These energy releases constitute a significant term in the energy balance of these quiescent volcanoes and can be used as baselines for energy release against which changes due to volcanic unrest can be compared.

6. Public health risk assessment

This study delineates important diffuse degassing areas extending below Furnas and Ribeira Quente villages. During the field work several inhabitants witnessed symptoms associated to high CO_2 concentrations during certain periods, as well as, the death of small animals (e.g., birds, chicken and cats) in some depressed areas. We also measured in some low ventilated trails CO_2 concentration at 20 cm above the ground as high as 80 vol.%.

Viveiros et al. [2009] revealed that even in areas where soil CO_2 degassing is low, variations in the meteorological variables (mainly barometric pressure and rainfall) may cause significant increases in the gas flux and create indoor hazardous conditions. In this work, it is considered that all houses over CO_2 degassing higher than 50 g m^{-2} d^{-1} may be at risk.

Previous studies [*Baxter et al*., 1999; *Sousa*, 2003] have estimated that about one third of Furnas village houses are located over important DDS. Considering a value of 50 g m^{-2} d^{-1}, used to delimit the DDS and as a possible threshold for the biological background flux, we estimate that 58% of the Furnas village houses are built over hydrothermal CO_2 degassing ground. This higher percentage may be explained by (1) more detailed sampling design, (2) lower threshold for hydrothermal CO_2 degassing and (3) construction of recent houses in the vicinities of Ribeira dos Tambores fumarolic field.

The diffuse degassing anomaly at Ribeira Quente village is shown here for the first time. We estimate that about 98% of the houses are placed over anomalous degassing areas, a scenario even worse than Furnas village. Based on these results, it is evident

that these degassing maps are important for health risk assessment studies and they should be taken into account by the land-use planners in any degassing area.

7. Conclusions

Different CO_2 sources are identified at Furnas volcano area based on the isotopic composition of CO_2 efflux [*Chiodini et al*., 2008] and GSA methodology [*Chiodini et al.*, 1998] that together contributed for a more accurate definition of a threshold for CO_2 biogenic background, fundamental to define the DDS, to estimate the hydrothermal CO_2 release, and as baseline for the interpretation of time variation of fluxes from the soil. Significant DDS were recognized at the volcano. The main DDS show NW-SE pattern, well correlated to the orientations of the main tectonic structures of the volcano, suggesting an evident structural control on degassing.

Hydrothermal CO_2 emissions by Furnas caldera and Ribeira Quente village area were estimated to be ~ 968 t d^{-1}. Several other diffuse degassing areas were detected along transects, but the morphology of the volcano did not allow to sample in a grid thereby making it impossible to estimate the gas emission for a larger area. To achieve a more complete evaluation of the CO_2 release by Furnas volcano future works are planned to calculate also the CO_2 emission other than diffuse degassing, namely from the fumaroles, steaming vents and Furnas lake.

The thermal energy release associated to the diffuse degassing at Furnas caldera was estimated to be ~ 118 MW for an area of ~ 4.8 km^2, which is in the same order of magnitude of the energy released in other quiescent volcanoes worldwide.

The present work enlarges significantly the area sampled in previous works, linking the main fumarolic fields from Furnas caldera. Despite small divergences, which can be attributed to the different sampling grids and changes in the physical proprieties of the soil (as for instance the permeability), the general degassing pattern seems to remain quite stable in the Furnas village area along the last 15 years. *Jones et al*. [1999], based

on the Furnas stratigraphy and statistical analysis of past eruptions, estimated a probability of 30% for the occurrence of an eruption in the next 100 years at Furnas volcano. Considering that there are urban settlements in and around the caldera, it is important to apply different monitoring techniques to characterize those parameters that should respond to occurrence of volcanic unrest. Due to the stability of the DDS along the time, these degassing maps may be useful for volcanic/seismic monitoring purposes as they may represent a reference for future variations on the state of activity of the volcano. Measurements performed in a regular fixed grid together with hourly data from the two permanent CO_2 flux stations installed in the volcano constitute a first proposal of a reliable monitoring system to detect any change in the diffuse degassing behavior inside Furnas caldera.

In what concerns a public health risk assessment perspective, it is noticed that 98% and 58% of houses at Ribeira Quente and Furnas village, respectively, are placed over hydrothermal CO_2 emanations. These high percentages of buildings in anomalous diffuse degassing zones show the importance of these maps in volcanic regions or in soil degassing prone areas resulting from other sources, since the CO_2 gas can easily introduce in buildings, as it was already shown in several works.

Acknowledgements

Fátima Viveiros and Catarina Silva are supported by a PhD grant from Fundo Regional da Ciência e Tecnologia, Região Autónoma dos Açores. The authors would like to thank Maria João Pereira for her help in Botanic from Furnas volcano. Helpful reviews were provided by Cynthia Werner and two anonymous reviewers.

Bibliography

Aiuppa, A., A. Caleca, C. Federico, S. Gurrieri, and M. Valenza (2004), Diffuse degassing of carbon dioxide at Somma-Vesuvius volcanic complex (Southern Italy) and its relation with regional tectonics, *J. Volcanol. Geotherm. Res.,* 133, 55-79.

Annunziatellis, A., G. Ciotoli, S. Lombardi, and F. Nolasco (2003), Short and long-term hazard: the release of toxic gases in the Albano Hills volcanic area (central Italy), *J. Geoch. Exploration*, 77, 93–108.

Bajracharya, R.M., R. Lal, and J.M. Kimble (2000), Diurnal and Seasonal CO_2–C Flux from Soil as Related to Erosion Phases in Central Ohio, *Soil Sci. Soc. Am. J*., 64, 286-293.

Barberi, F., M. L. Carapezza, M. Ranaldi, and L. Tarchini (2007), Gas blowout from shallow boreholes at Fiumicino (Rome): induced hazard and evidence of deep CO_2 degassing on the Tyrrhenian margin of Central Italy, *J. Volcanol. Geotherm. Res.,* 165, 17-31.

Baubron, J. C., P. Baxter, R. Coutinho, P. Allard, T. Ferreira, and J. L. Gaspar (1994), Methodology for the drawing up of the Furnas Gas Hazard Map. In Barberi, F.; Casale, R. e Fratta, M. (Eds.) *The European laboratory volcanoes. Workshop proceedings*, Catania, 18 – 21 June.

Baubron, J. C., A. Rigo, and J. P. Toutain (2002), Soil gas profiles as a tool to characterise active tectonics areas: the Jaut Pass example (Pyrenees, France), *Earth Planet. Sci. Lett.*, 196, 69-81.

Baxter, P., J. C. Baubron, and R. Coutinho (1999), Health hazards and disaster potential of ground gas emissions at Furnas Volcano, São Miguel, Azores, *J. Volcanol. Geotherm. Res.,* 92, 95-106.

Beaubien, S. E., G. Ciotoli, and S. Lombardi (2003), Carbon dioxide and radon gas hazard in the Alban Hills area (central Italy), *J. Volcanol. Geotherm. Res*., 123, 63-80.

Bergfeld, D., F. Goff, and C. J. Janik (2001), Elevated carbon dioxide flux at the Dixie Valley geothermal field, Nevada; relations between surface phenomena and the geothermal reservoir, *Chem. Geol*., 177, 43-66.

Booth, B., R. Croasdale, and G. Walker (1978), A quantitative study of five thousand years of volcanism on São Miguel, Azores, *Philos. Trans. R. Soc. London.*, 288, 271-319.

Brombach, T., J. Hunzikerm, G. Chiodini, C. Cardellini, and L. Marini (2001), Soil diffuse degassing and thermal energy fluxes from the southern Lakki plain, Nisyros (Greece). *Geophys. Res. Lett.*, 28(1), 69–72.

Bruno, N., T. Caltabiano, S. Giammanco, and R. Romano (2001), Degassing of SO_2 and CO_2 at Mount Etna (Sicily) as an indicator of pre-eruptive ascent and shallow emplacement of magma, *J. Volcanol. Geotherm. Res.*, 110, 137-153.

Caliro, S., G. Chiodini, D. Galluzzo, D. Granieri, M. La Rocca, and G. Ventura (2005), Recent activity of Nisyros volcano (Greece) inferred from structural, geochemical and seismological data, *Bull. Volcanol.,* 67, 358-369, doi: 10.1007/s00445-004-0381-7.

Caracausi, A., R. Favara, S. Giammanco, F. Italiano, A. Paonita, G. Pecoraino, A. Rizzo, and P. M. Nuccio (2003), Mount Etna: Geochemical signals of magma ascent and unusually extensive plumbing system, *Geophys. Res. Lett*., 30(2), 1057, doi:10.1029/2002GL015463.

Carapezza, M.L., and D. Granieri (2004), CO_2 soil flux at Vulcano (Italy): comparison between active and passive methods. *Appl. Geochem*., 19, 73-88.

Carapezza, M. L., S. Inguaggiato, L. Brusca, and M. Longo (2004), Geochemical precursors of the activity of an open-conduit volcano: The Stromboli 2002–2003 eruptive events, *Geophys. Res. Lett*., 31, L07620, doi:10.1029/2004GL019614.

Carapezza, M. L., T. Ricci, M. Ranaldi and L. Tarchini (2009), Active degassing structures of Stromboli and variations in diffuse CO_2 output related to the volcanic activity, *J. Volcanol. Geotherm. Res.,* 182, 231-245.

Cardellini, C, G. Chiodini, and F. Frondini (2003), Application of Stochastic Simulation to CO_2 flux from soil: Mapping and Quantification of Gas Release. *J. Geophys. Res*., 108(B9), 2425-2437, doi:10.1029/2002JB002165.

Carmo, R. (2004), *Geologia estrutural da região Povoação - Nordeste (ilha de S. Miguel, Açores).* Masther Thesis, University of the Azores, 121pp. (in Portuguese).

Census (2001), Instituto Nacional de Estatística, Recenseamento Geral da População e Habitação. Portugal, (in Portuguese).

Cheng, W. (1996). Measurement of rhizosphere respiration and organic matter decomposition using natural ^{13}C, *Plant. Soil*., 183, 263–268.

Chiodini, G., A. Baldini, F. Barberi, M. L. Carapezza, C. Cardellini, F. Frondini, D. Granieri, and M. Ranaldi (2007), Carbon dioxide degassing at Latera caldera (Italy): Evidence of geothermal reservoir and evaluation of its potential energy, *J. Geophys. Res.*, 112, B12204, doi:10.1029/2006JB004896.

Chiodini, G., C. Cardellini, A. Amato, E. Boschi, S. Caliro, F. Frondini, and G. Ventura (2004), Carbon dioxide Earth degassing and seismogenesis in central and southern Italy, *Geophys. Res. Lett.,* 31, L07615, doi:10.1029/2004GL019480.

Chiodini, G., D. Granieri, R. Avino, S. Caliro, A. Costa, and C. Werner (2005), Carbon dioxide diffuse degassing and estimation of heat release from volcanic and hydrothermal systems, *J. Geophys. Res.*, 110, B08204, doi:10.1029/2004JB003542.

Chiodini, G., F. Frondini, C. Cardellini, D. Granieri, L. Marini, and G. Ventura (2001), CO_2 degassing and energy release at Solfatara volcano, Campi Flegrei, Italy, *J. Geophys. Res.*, 106, 16213-16221.

Chiodini, G., R. Avino, T. Brombach, S. Caliro, C. Cardellini, S. De Vita, F. Frondini, E. Marotta, and G. Ventura (2004), Fumarolic degassing west of Mount Epomeo, Ischia (Italy), *J. Volcanol. Geotherm. Res.*, 133, 291-309.

Chiodini, G., R. Cioni, M. Guidi, B. Raco, and L. Marini (1998), Soil CO_2 flux measurements in volcanic and geothermal areas, *Appl. Geochem.*, 13, 543-552.

Chiodini, G., S. Caliro, C. Cardellini, R. Avino, D. Granieri, and A. Schmidt (2008), Carbon isotopic composition of soil CO_2 efflux, a powerful method to discriminate different sources feeding soil CO_2 degassing in volcanic-hydrothermal areas, *Earth Planet. Sci. Lett.,* 274 (3-4), 372-379.

Chiodini, G., T. Brombach, S. Caliro, C. Cardellini, L. Marini, and W. Dietrich (2002), Geochemical evidences of an ongoing volcanic unrest at Nisyros Island (Greece), *Geophys. Res. Lett*., 29 (16), 1759, doi 10.1029/2001GL014355.

Cole, P., G. Queiroz, N. Wallenstein, J. L. Gaspar, A. Duncan, and J. Guest (1995), An historic subplinian/phreatomagmatic eruption: the 1630 AD eruption of Furnas volcano, São Miguel, Azores, *J. Volcanol. Geotherm. Res.,* 69, 117-135.

Costa, A. (2006), *Atlas hidrogeológico das águas minerais dos Açores*. Masther Thesis, University of the Azores, 146 p. (in Portuguese).

Cruz, J. V., P. Antunes, C. Amaral, Z. França, and J. C. Nunes (2006), Volcanic Lakes from Azores Archipelago (Portugal): Geological setting and geochemical characterization, *J. Volcanol. Geotherm. Res.*, 156, 135-157.

Cruz, J. V., R. Coutinho, M. R. Carvalho, N. Óskarsson, and S. R. Gislason (1999), Chemistry of waters from Furnas Volcano, São Miguel, Azores: fluxes of volcanic carbon dioxide and leached material, *J. Volcanol. Geotherm. Res.,* 92, 151-167.

David, M. (1977), *Geostatistical Ore Reserve Estimation*. 364pp. Elsevier Scientific Publishing Company, Amsterdam.

Deutsch, C.V., Journel, A.G., 1998. *GSLIB: Geostatistical Software Library and User's Guide*. 369pp. Applied Geostatistics Series. Oxford Univerity Press, New York Oxford.

Farrar, C. D., M. L. Sorey, W. C. Evans, J. F. Howle, B. D. Kerr, B. M. Kennedy, C.-Y. King, and J. R. Southon (1995), Forest-killing diffuse CO_2 emission at Mammoth Muntain as a sign of magmatic unrest, *Nature*, 376, 675-678.

Ferreira, T., J. L. Gaspar, F. Viveiros, M. Marcos, C. Faria, and F. Sousa (2005), Monitoring of fumarole discharge and CO_2 soil degassing in the Azores: contribution to volcanic surveillance and public health risk assessment. *Ann. Geophys*., 48 (4-5), 787-796.

Ferreira, T., and N. Óskarsson (1999), Chemistry and isotopic composition of fumarole discharges of Furnas caldera, *J. Volcanol. Geotherm. Res.,* 92, 169-179.

Fridriksson, T., B. R. Kristjánsson, H. Ármannsson, E. Margrétardóttir, S. Ólafsdóttir, and G. Chiodini (2006), CO_2 emissions and heat flow through soil, fumaroles, and steam heated mud pools at the Reykjanes geothermal area, SW Iceland, *Appl. Geochem*., 21, 1551-1569.

Frondini, F., G. Chiodini, S. Caliro, C. Cardellini, D. Granieri, and G. Ventura (2004), Diffuse CO_2 degassing at Vesuvio, Italy, *Bull. Volcanol*. 66 (2004), 642–651.

Gaspar, J. L., T. Ferreira, G. Queiroz, N. Wallenstein, J. Pacheco, J. Guest, A. M. Duncan, and P. Cole (1995), Evolução morfoestrutural do Vulcão das Furnas (ilha de S. Miguel, Açores). *Memórias,* 4, Museu e Laboratório Mineralógico e Geológico, Faculdade de Ciências, Universidade do Porto, 999-1003 (in Portuguese).

Gerlach, T. M., M. P. Doukas, K. A. McGee, and R. Kessler (1998), Three-year decline of magmatic CO_2 emissions from soils of a Mammoth Mountain tree kill: Horseshoe Lake, CA, 1995-1997, *Geophys. Res. Lett*., 25(11), 1947–1950.

Giammanco, S., S. Gurrieri, and M. Valenza (1998), Anomalous soil CO_2 degassing in relation to faults and eruptive fissures on Mount Etna (Sicily, Italy), *Bull. Volcanol.*, 60, 252-259.

Giammanco, S., S. Gurrieri, and M. Valenza (2006), Fault-controlled soil CO_2 degassing and shallow magma bodies: summit and lower east rift of Kilauea volcano (Hawaii), 1997, *Pure Appl. Geophys.*, 163, 853-867.

Granieri, D., G. Chiodini, W. Marzocchi, and R. Avino (2003), Continuous monitoring of CO_2 soil diffuse degassing at Phlegraean Fields (Italy): influence of environmental and volcanic parameters, *Earth Planet. Sci. Lett.*, 212, 167-179.

Granieri, D., M. L. Carapezza, G. Chiodini, R. Avino, S. Caliro, M. Ranaldi, T. Ricci, and L. Tarchini (2006), Correlated increase in CO_2 fumarolic content and diffuse emission from La Fossa crater (Vulcano, Italy): Evidence of volcanic unrest or increasing gas release from a stationary deep magma body?, *Geophys. Res. Lett.*, 33, L13316, doi:10.1029/2006GL026460.

Guest, J., J. L. Gaspar, P. D. Cole, G. Queiroz, A. M. Duncan, N. Wallenstein, T. Ferreira, and J. M. Pacheco (1999), Volcanic geology of Furnas Volcano, São Miguel, Azores, *J. Volcanol. Geotherm. Res.,* 92, 1-29.

Hernández, P. A., J. M. Salazar, Y. Shimoike, T. Mori, K. Notsu, and N. Perez (2001a) Diffuse emission of CO_2 from Miyakejima volcano, Japan, *Chem. Geol.*, 177, 175–185.

Hernández, P. A., K. Notsu, J. M. Salazar, T. Mori, G. Natale, H. Okada, G. Virgili, Y. Shimoike, M. Sato, and N. M. Pèrez (2001b), Carbon dioxide degassing by advective flow from Usu Volcano, Japan, *Science,* 292, 83-86.

Hernández, P., K. Notsu, M. Tsurumi, T. Mori, M. Ohno, Y. Shimoike, J. Salazar, and N. Pérez (2003), Carbon dioxide emissions from soils at Hakkoda, north Japan, *J. Geophys. Res*., 108(B4), 2210, doi:10.1029/2002JB001847.

Hernández, P. A., N. M. Pérez, J. M. Salazar, S. Nakai, K. Notsu, and H. Wakita (1998), Diffuse emission of carbon dioxide, methane, and helium-3 from Teide Volcano, Tenerife, Canary Islands, *Geophys. Res. Lett*., 25(17), 3311–3314.

Jones, G., D. K. Chester, and F. Shooshtarian, 1999: Statistical analysis of the frequency of eruptions at Furnas Volcano, São Miguel, Azores. *J. Volcanol. Geotherm. Res*., 92, 31-38.

Keenan, J. H., F. G. Keyes, P. G. Hill, and J. G. Moore (1969), *Steam Tables: Thermodynamic Properties of Water Including Vapor, Liquid, and Solid Phases*, John Wiley, Hoboken, N. J., 162 pp.

Kerrick, D.M, (2001), Present and past non-anthropogenic CO_2 degassing from the solid Earth. *Rev. Geophys*, 39, 565-585.

Lan, T. F., T. F. Yang, H.-F. Lee, Y.-G. Chen, C.-H. Chen, S.-R. Song, and S. Tsao (2007), Compositions and flux of soil gas in Liu-Huang-Ku hydrothermal area, northern Taiwan, *J. Volcanol. Geotherm.* Res., 165, 32-45.

Lewicki, J. L., C. Connor, K. St-Amand, J. Stix, and W. Spinner (2003), Self-potential, soil CO_2 flux, and temperature on Masaya volcano, Nicaragua, *Geophys. Res. Lett*., 30(15), 1817, doi:10.1029/2003GL017731.

Lewicki, J. L., D. Bergfeld, C. Cardellini, G. Chiodini, D. Granieri, N. Varley, and C. Werner (2005), Comparative soil CO_2 flux measurements and geostatistical estimation methods on Masaya volcano, Nicaragua, *Bull. Volcanol.*, 68, 76-90, doi:10.1007/s00445-005-0423-9.

Machado, F. (1959), Submarine pits of the Azores plateau. *Bull. Volcanol*., II(XXI), 109-116.

Madeira, J., and A. Ribeiro (1990), Geodinamic models for the Azores triple junction: a contribution from tectonics. *Tectonophys*., 184, 405-415.

Marques, R., J. Zêzere, R. Trigo, J. Gaspar, and I. Trigo (2007), Rainfall patterns and critical values associated with landslides in Povoação County (São Miguel Island, Azores): relationships with the North Atlantic Oscillation. *Hydrol. Process*, 22, 478-494, doi:10.1002/hyp.6879.

Moore, R. (1990), Volcanic geology and eruption frequency, São Miguel, Azores, *Bull. Volcanol*., 52, 602-614.

Morner, N.-A. and G. Etiope (2002), Carbon degassing from the lithosphere. *Glob. Planet. Change*, 33(1-2), 185-203.

Nakadai, T., M. Yokozawa, H. Ikeda, and H. Koizumi (2002), Diurnal changes of carbon dioxide flux from bare soil in agricultural field in Japan. *Appl. Soil Ecol*. 19, 161–171.

Norman, J. M., R. Garcia, and S. B. Verma (1992), Soil Surface CO_2 Fluxes and the Carbon Budget of a Grassland, *J. Geophys. Res.*, 97(D17), 18845–18853.

Notsu, K., K. Sugiyama, M. Hosoe, A. Uemura, Y. Shimoike, F. Tsunomori, H. Sumino, J. Yamamoto, T. Mori, and P. A. Hernández (2005), Diffuse CO_2 efflux from Iwojima volcano, Izu-Ogasawara arc, Japan, *J. Volcanol. Geotherm. Res.*, 139, 147-161.

Padrón, E., P. A. Hernandéz, T. Toulkeridis, N. M. Pérez, R. Marrero, G. Melián, G. Virgili, and K. Notsu (2008), Diffuse CO_2 emission rate from Pululahua and the lake-filled Cuicocha calderas, Ecuador, *J. Volcanol. Geotherm. Res.*, 176, 163-169.

Pruess, K. (1991), TOUGH2: A general purpose numerical simulator for multiphase fluid and heat flow, *Rep. LBL 29400*, Lawrence Berkeley Natl. Lab., Berkeley, Calif.

Queiroz, G., J. L. Gaspar, P. Cole, J. Guest, N. Wallenstein, A. M. Duncan, and J. Pacheco (1995), Erupções vulcânicas no Vale das Furnas (ilha de S. Miguel, Açores) na primeira metade do século XV, *Açoreana*, 8 (1), 159-165 (in Portuguese).

Raich, J. W. and W. H. Schlesinger (1992), The global carbon dioxide flux in soil respiration and its relationship to vegetation and climate, *Tellus*, 44B, 81-99.

Raich, J. W. and A. Tufekcioglu (2000), Vegetation and soil respiration: Correlations and controls. *Biogeochem.*, 48(1), 71-90.

Reed, G. F., L. Freyja, and B. D. Meade (2002), Use of Coefficient of Variation in Assessing Variability of Quantitative Assays, *Clin. Diagn. Lab. Immunol.*, 9 (6), 1235–1239, doi: 10.1128/CDLI.9.6.1235–1239.2002.

Revil, A., A. Finizola, S. Piscitelli, E. Rizzo, T. Ricci, A. Crespy, B. Angeletti, M. Balasco, S. Barde Cabusson, L. Bennati, A. Bolève, S. Byrdina, N. Carzaniga, F. Di Gangi, J. Morin, A. Perrone, M. Rossi, E. Roulleau, B. Suski (2008), Inner structure of La Fossa di Vulcano (Vulcano Island, southern Tyrrhenian Sea, Italy) revealed by high-resolution electric resistivity tomography coupled with self-potential, temperature, and CO_2 diffuse degassing measurements, *J. Geophys. Res.*, 113, B07207, doi:10.1029/2007JB005394.

Salazar, J. M. L., P. A. Hernández, N. M. Pérez, G. Melián, J. Álvarez, F. Segura, and K. Notsu (2001), Diffuse emission of carbon dioxide from Cerro Negro Volcano, Nicaragua, Central America, *Geophys. Res. Lett.*, 28(22), 4275–4278.

Searle, R. (1980), Tectonic pattern of the Azores spreading centre and triple junction. *Earth Planet. Sci. Lett.*, 51, 415-434.

Shimoike, Y., K. Kazahaya, and H. Shinohara (2002), Soil gas emission of volcanic CO_2 at Satsuma-Iwojima volcano, Japan, *Earth Planets Space*, 54, 239–247.

Silveira, D., J. L. Gaspar, T. Ferreira, and G. Queiroz (2003), Reassessment of the historical seismic activity with major impact on S. Miguel Island (Azores). *Natural Haz. Earth Sys. Sci.*, 3, 1-8.

Sinclair, A. J. (1974), Selection of threshold values in geochemical data using probability graphs, *J. Geochem. Explor.*, 3, 129–149.

Sorey, M. L., W. C. Evans, B. M. Kennedy, C. D. Farrar, L. J. Hainsworth, and B. Hausback (1998), Carbon dioxide and helium emissions from a reservoir of magmatic gas beneath Mammoth Mountain, California, *J. Geophys. Res.*, 103(B7), 15,303–15,323.

Sousa, F. (2003), *Cartografia de anomalias geoquímicas associadas a processos de desgaseificação difusa no Vulcão das Furnas (S. Miguel, Açores): contribuição para a avaliação de riscos vulcânicos*. Masther Thesis, University of the Azores, 106p. (in Portuguese).

Toutain, J. P., and J. C. Baubron (1999), Gas geochemistry and seismotectonics: a review, *Tectonophys*., 304, 1–27.

Valadão, P., J. L. Gaspar, G. Queiroz, and T. Ferreira (2002), Landslides density map of S. Miguel island, Azores archipelago, *Natural Haz. Earth Sys. Sci.*, 2, (1/2), 51-56.

Viveiros, F., T. Ferreira, J. Cabral Vieira, C. Silva, and J. L. Gaspar (2008), Environmental influences on soil CO2 degassing at Furnas and Fogo volcanoes (São Miguel Island, Azores archipelago), *J. Volcanol. Geotherm. Res.*, 177, 883-893.

Viveiros, F., T. Ferreira, C. Silva and J. L. Gaspar (2009), Meteorological factors controlling soil gases and indoor CO_2 concentration: a permanent risk in degassing areas. *Sci. Total Environ*. 407, 1362-1372.

Vogt, P. R. and W.Y. Jung (2004), The Terceira rift as hyper-slow, hotspot dominated oblique spreading axis: a comparison with other slow-spreading plate boundaries, *Earth Planet. Sci. Lett*., 218, 77–90.

Werner, C. and C. Cardellini (2006), Comparison of carbon dioxide emissions with fluid upflow, chemistry, and geologic structures at the Rotorua geothermal system, New Zealand, *Geothermics*, 35, 221-238.

Werner, C., and S. Brantley (2003), CO_2 emissions from the Yellowstone volcanic system, *Geochem. Geophys. Geosyst.*, 4(7), 1061, doi:10.1029/2002GC000473, 2003.

Werner, C., S. Hurwitz, W. C. Evans, J. B. Lowenstern, D. Bergfeld, H. Heasler, C. Jaworowski and A. Hunt (2008), Volatile emissions and gas geochemistry of Hot Spring Basin, Yellowstone National Park, USA, *J. Volcanol. Geotherm. Res.*, 178, 751-762.

Werner, C., S. L. Brantley, and K. Boomer (2000), CO_2 emissions related to the Yellowstone volcanic system. Statistical sampling, total degassing, and transport mechanisms, *J. Geophys. Res.*, 105, 10831-10846.

Captions

Figure 1. (a) Azores archipelago location with the main tectonic structures; (b) São Miguel island digital elevation model with location of the main active volcanic systems: 1 – Sete Cidades volcano; 2 – Picos Waist Zone; 3 – Fogo volcano; 4 – Achada das Furnas Plateau ; 5 - Furnas volcano; (c) Main volcano-tectonic structures (based on aerial photography visualization and information collected from *Cole et al*., 1995; *Gaspar et al*., 1995; *Guest et al*., 1999; *Carmo*, 2004) and hydrothermal manifestations at Furnas volcano. CO_2 cold springs and thermal springs are identified according to the work of *Costa* [2006]. Steam emissions were mapped during this work. Legend: 1 - Furnas lake fumarolic field; 2 - Furnas village fumarolic field; 3 - Ribeira dos Tambores fumaroles. (Contour lines are spaced 50 m; Datum=WGS84).

Figure 2. Soil CO_2 concentration maps from Furnas village according to (a) *Baubron et al*. [1994] and (b) *Sousa* [2003]. Geomorphologic features legend according to Figure 1c.

Figure 3. (a) Location of the sampling points at Furnas volcano. B, C and D squares represent Furnas lake, Furnas village and Ribeira Quente village subsets. Detailed sampling network for (b) Furnas lake fumarolic field and (c) Furnas village fumaroles. P1-P1' transect represents the CO_2 profile shown in Figure 9.

Figure 4. Probability plot of soil CO_2 flux at Furnas volcano (data referenced as A1, Table 1) and outside Furnas area (data referenced as E, Table 1).

Figure 5. Diagram plotting soil CO_2 efflux (g m^{-2} d^{-1}) and carbon isotopic composition of soil CO_2 efflux (‰). Only samples with soil CO_2 efflux lower than 1400 g m^{-2} d^{-1} are represented and compared with theoretical lines that represent light and heavy CO_2 sources with different efflux rates.

Figure 6. Experimental and modeled variograms of the soil CO_2 flux normal scores for the different data sets. Legend: Cc (sill); a (range, m).

Figure 7. E-type soil CO_2 flux map for Furnas caldera and Ribeira Quente village (cell size = 10 x 10 m). Transects performed across volcanic structures do not allow to perform interpolations and single points are represented with graded colors. Uppercase letters represent DDS at Furnas caldera as mentioned in the text. Geomorphologic and tectonic features legend is the same as Figure 1c.

Figure 8. Probability maps for soil CO_2 flux at Furnas caldera (a) and Ribeira Quente village (b). The color scale shows the probability of soil CO_2 flux exceeding 50 g m^{-2} d^{-1}. Geomorphologic and tectonic features legend is the same as Figure 1c. The letters A through G refer to specific degassing locations as mentioned in the text.

Figure 9. CO_2 profile performed across Furnas caldera. The grey shadow represents the topography and the black line the soil CO_2 flux values. Profile location is displayed in Figure 3 and is oriented from P1 to P1'.

Figure 10. E-type soil CO_2 flux maps for Furnas village fumaroles and Furnas lake fumarolic fields based on the detailed survey (a; c) and in the Furnas caldera global sampling (b; d). Geomorphologic features and hydrothermal manifestations follow legend of Figure 1c. Soil CO_2 flux graded scale is the same of Figure 7 (cell size = 3 x 3 m and contour lines are spaced 5 m).

Table 1. Descriptive statistics of flux data. Asterisk (*) indicates A1 data and includes all data from Furnas caldera (A2) and some measurements performed along profiles.

Table 2. Soil CO_2 flux and $\delta^{13}C$-values of the associated CO_2. Sampled point number 13 corresponds to a sample of Caldeira Grande fumarole. Legend: n.d. = not detected.

Table 3. Statistical parameters from the partitioned CO_2 flux populations and the 90% confidence intervals of the mean at Furnas volcano.

Table 4. Total CO_2 output and uncertainties derived from 100 sGs realizations. The asterisk (*) identifies subsets of data extracted from the Furnas caldera map. Ref. designations establish correspondence to data sets defined in Table 1.

Table 5. CO_2 diffuse degassing emitted by several degassing areas around the world. The areas are sorted based on the CO_2 emission km^{-2}.

Table 1. Descriptive statistics of flux data. Asterisk (*) indicates A1 data and includes all data from Furnas caldera (A2) and some measurements performed along profiles.

Study area	Ref.	Number of points	Sampling strategy	Area (km^2)	Mean ($g\ m^{-2}\ d^{-1}$)	Median ($g\ m^{-2}\ d^{-1}$)	Minimum ($g\ m^{-2}\ d^{-1}$)	Maximum ($g\ m^{-2}\ d^{-1}$)	Skewness
Furnas volcano*	A1	1756	Irregular	-	363	30	0	> 25000	10
Furnas caldera	A2	1362	Irregular	5.80	371	33	0	> 25000	9
Furnas lake fumaroles	B	367	7 - 10 m grid	0.04	325	37	2	20579	10
Furnas village fumaroles	C	334	5 - 7 m grid	0.04	630	110	1	19469	7
Ribeira Quente village	D	148	Irregular	0.35	582	34	1	> 25000	8
Outside Furnas volcano	E	88	Irregular	-	15	17	0	34	0

Table 2. Soil CO_2 flux and $\delta^{13}C$-values of the associated CO_2. Sampled point number 13 corresponds to a sample of Caldeira Grande fumarole. Legend: n.d. = not detected.

Reference	Easting WGS84 (m)	Northing WGS84 (m)	CO_2 concentration (ppm)	Soil CO_2 flux (g m^{-2} d^{-1})	$\delta^{13}C$ efflux (‰ vs. PBD)	Soil temperature (ºC)
1	649294	4181930	1198	20	-12.28	24
2	648751	4181917	1062	29	-11.69	24
3	649160	4182022	1320	49	-11.37	24
4	649248	4181700	6893	290	-7.97	25
5	649069	4181978	2233	105	-7.88	24
6	647059	4181556	4524	205	-6.16	24
7	648044	4181517	4226	148	-5.50	23
8	647169	4181543	n.d.	> 25000	-4.42	98
9	649349	4181994	6438	200	-4.39	31
10	649374	4181890	40935	1178	-4.23	86
11	649492	4182008	n.d.	3573	-3.94	n.d.
12	649373	4181889	36152	2452	-3.11	53
13	649354	4181940	n.d.	n.d.	-4.26	n.d.

Table 3. Statistical parameters from the partitioned CO_2 flux populations and the 90% confidence intervals of the mean at Furnas volcano.

Population	**CO_2 source**	**Proportion (%)**	**Mean CO_2 flux (g m^{-2} d^{-1})**	**Mean CO_2 90% confidence interval**
Aa	-	2	2.3	1.9 - 3.1
Ab	Mainly biogenic	76	32	31 - 37
Ac	Hydrothermal	22	535	411 - 727

Table 4. Total CO_2 output and uncertainties derived from 100 sGs realizations. The asterisk (*) identifies subsets of data extracted from the Furnas caldera map. Ref. designations establish correspondence to data sets defined in Table 1.

Study Area	Ref.	Area (km^2)	Number of points	Number of points km^{-2}	Mean CO_2 flux (t d^{-1}) (± S.D.)	CO_2 flux (t km^{-2} d^{-1})	Emission rate range (t d^{-1})	Hydrothermal CO_2 flux (t d^{-1})	Coefficent of variation (%)
Furnas caldera	A2	5.85	1362	233	959 (±84)	164	745 - 1227	734	9
Furnas lake fumaroles	B	0.043	367	8507	14 (±2)	325	11 - 19	13	14
Furnas lake fumaroles*	A2.1	0.043	37	864	47 (±15)	1093	26 - 104	-	32
Furnas village fumaroles	C	0.038	334	8817	17 (±2)	447	14 - 22	16	12
Furnas village fumaroles*	A2.2	0.038	65	1716	64 (±12)	1684	39 - 107	-	19
Ribeira Quente Village	D	0.350	148	423	243 (±43)	694	160 - 390	234	18

Table 5. CO_2 diffuse degassing emitted by several degassing areas around the world. The areas are sorted based on the CO_2 emission km^{-2}.

Study area	CO_2 flux ($t\ d^{-1}$)	Area (km^2)	Number of points	Number of points km^{-2}	CO_2 flux ($t\ km^{-2}\ d^{-1}$)	Reference
Cuicocha caldera, Ecuador	106	13.30	172	13	8	*Padròn et al*., 2008
Pululahua caldera, Ecuador	270	27.60	217	8	10	*Padròn et al*., 2008
Satsuma-Iwojma volcano, Japan	80	2.50	155	62	32	*Shimoike et al*., 2002
Iwojima Volcano, Japan	760	22.00	272	12	35	*Notsu et al*., 2005
Vesuvio Volcano, Italy	193.8	5.50	636	116	35	*Frondini et al*., 2004
Mt. Epomeo, Italy	32.6	0.86	336	391	38	*Chiodini et al*., 2004
Vulcano Island, Italy	75	1.90	423	223	39	*Chiodini et al*., 1998
Nisyros caldera, Greece	84	2.00	2883	1442	42	*Cardellini et al*., 2003
Yanbajain geothermal field, China	138	3.20	331	103	43	*Chiodini et al*., 1998
Nea Kameni Island, Greece	15.4	0.28	63	225	55	*Chiodini et al*., 1998
Reykjanes geothermal area, Iceland	13.5	0.22	352	1600	61	*Fridriksson et al*., 2006
Taupo Volcanic Zone, New Zealand	620	8.90	956	107	70	*Werner and Cardellini*, 2006
Miyakejima Volcano (summit), Japan	100 - 150	0.60	~ 70	117	167	*Hernández et al*., 2001a
Hakkoda region, Japan	127	0.58	180	310	219	*Hernández et al*., 2003
Methana volcanic system, Greece	2.59	0.01	39	3900	259	*D'Alessandro et al*., 2008
Poggio dell'Olivo, Italy	233.5	0.82	196	239	285	*Cardellini et al*., 2003
Hot Spring Basin, Yellowstone, USA	60	0.16	228	1471	387	*Werner et al*., 2008
Mud Volcano, Yellowstone, USA	1730	3.50	410	117	494	*Werner et al*., 2000
Liu-Huang-Ku, Taiwan	22.4	0.03	163	4794	659	*Lan et al*., 2007
Teide Volcano (Summit), Spain	380	0.53	100	189	717	*Hernández et al*., 1998
Horseshoe Lake, USA	104.3	0.13	313	2408	802	*Cardellini et al*., 2003
Solfatara Volcano, Italy	1500	1.00	333	333	1500	*Chiodini et al*., 2001
Cerro Negro Volcano, Nicaragua	2800	0.58	220	379	4828	*Salazar et al*., 2001

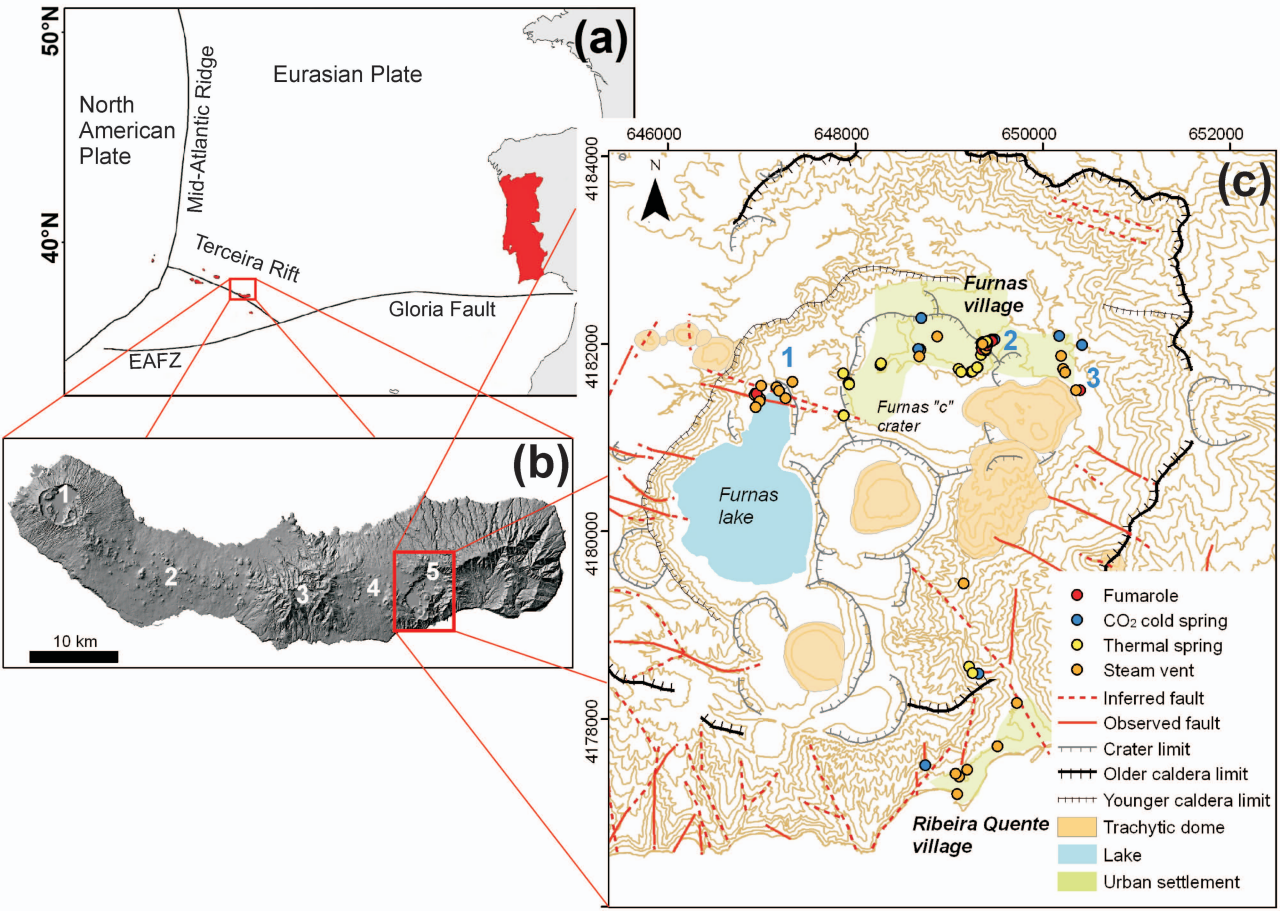
(a)
50°N
40°N
North American Plate
Eurasian Plate
Mid-Atlantic Ridge
Terceira Rift
Gloria Fault
EAFZ
(b)
1
2
3
4
5
10 km
(c)
646000
648000
650000
652000
4184000
4182000
4180000
4178000
N
Furnas village
Furnas "c" crater
Furnas lake
Ribeira Quente village
Fumarole
CO2 cold spring
Thermal spring
Steam vent
Inferred fault
Observed fault
Crater limit
Older caldera limit
Younger caldera limit
Trachytic dome
Lake
Urban settlement

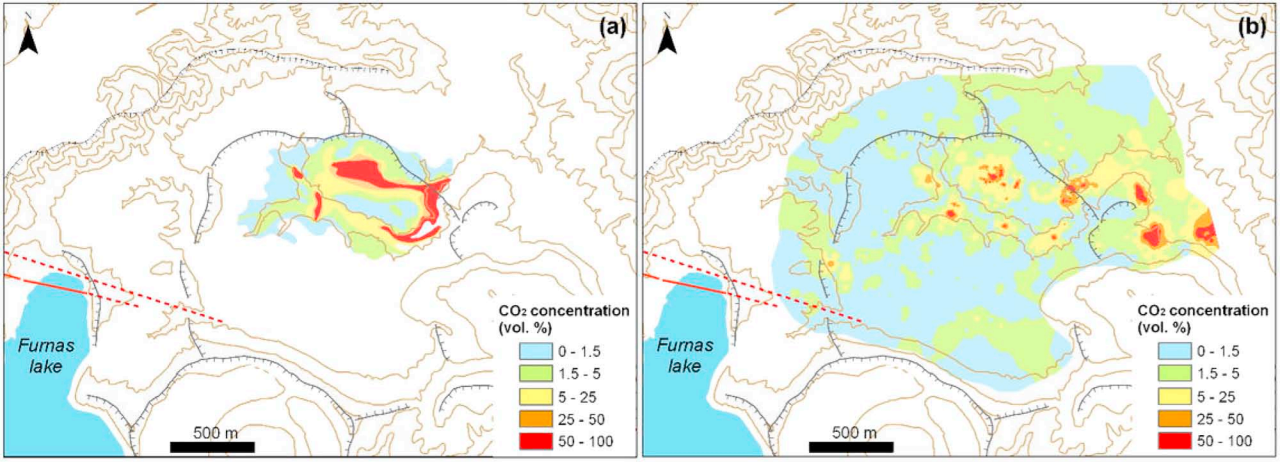
(a)
Furnas lake
500 m
CO2 concentration (vol. %)
0 - 1.5
1.5 - 5
5 - 25
25 - 50
50 - 100
(b)
Furnas lake
500 m
CO2 concentration (vol. %)
0 - 1.5
1.5 - 5
5 - 25
25 - 50
50 - 100

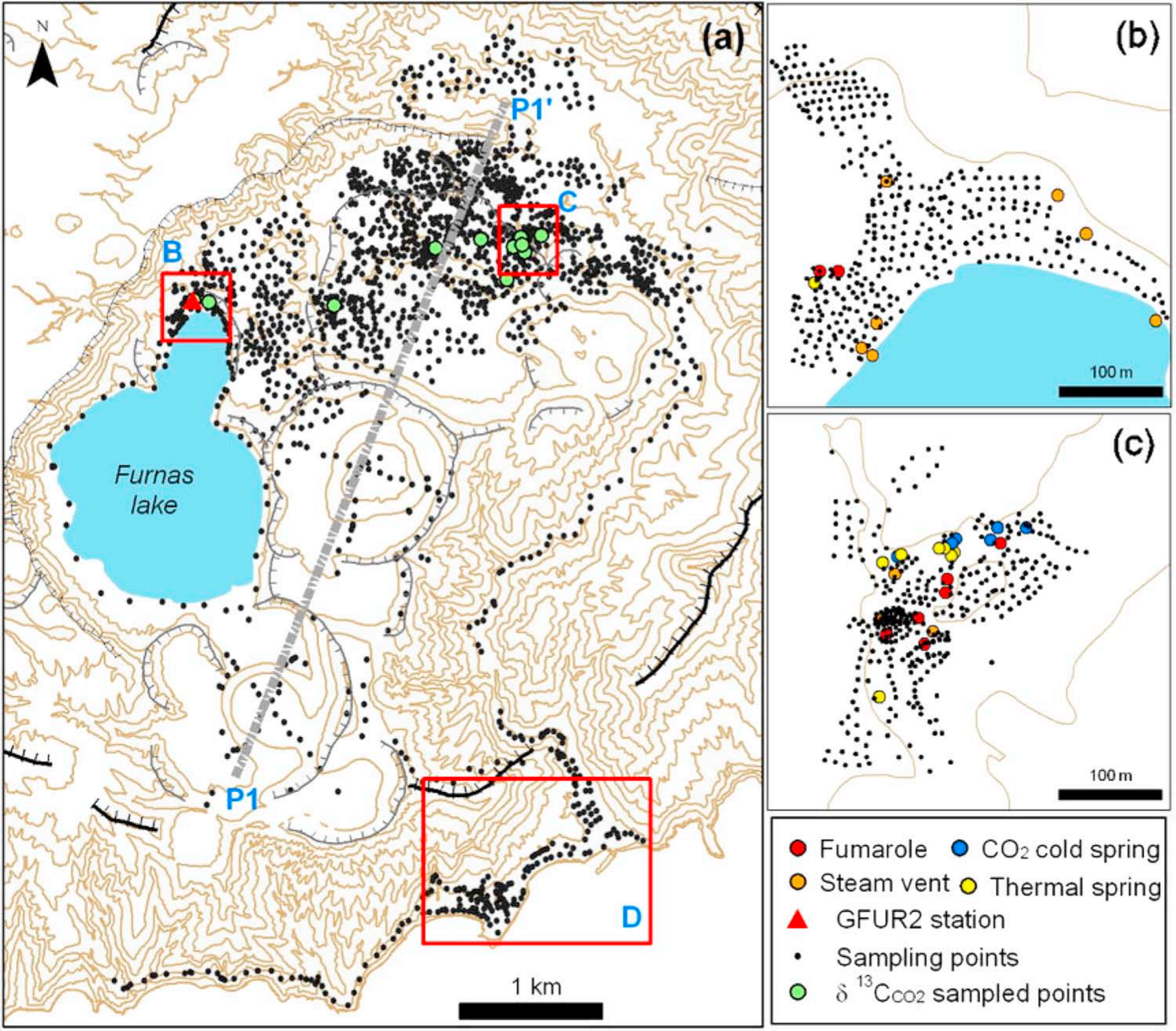
(a)
N
P1'
C
B
Furnas
lake
P1
D
1 km
(b)
100 m
(c)
100 m
Fumarole
CO_2 cold spring
Steam vent
Thermal spring
GFUR2 station
Sampling points
$\delta\ ^{13}C_{CO2}$ sampled points

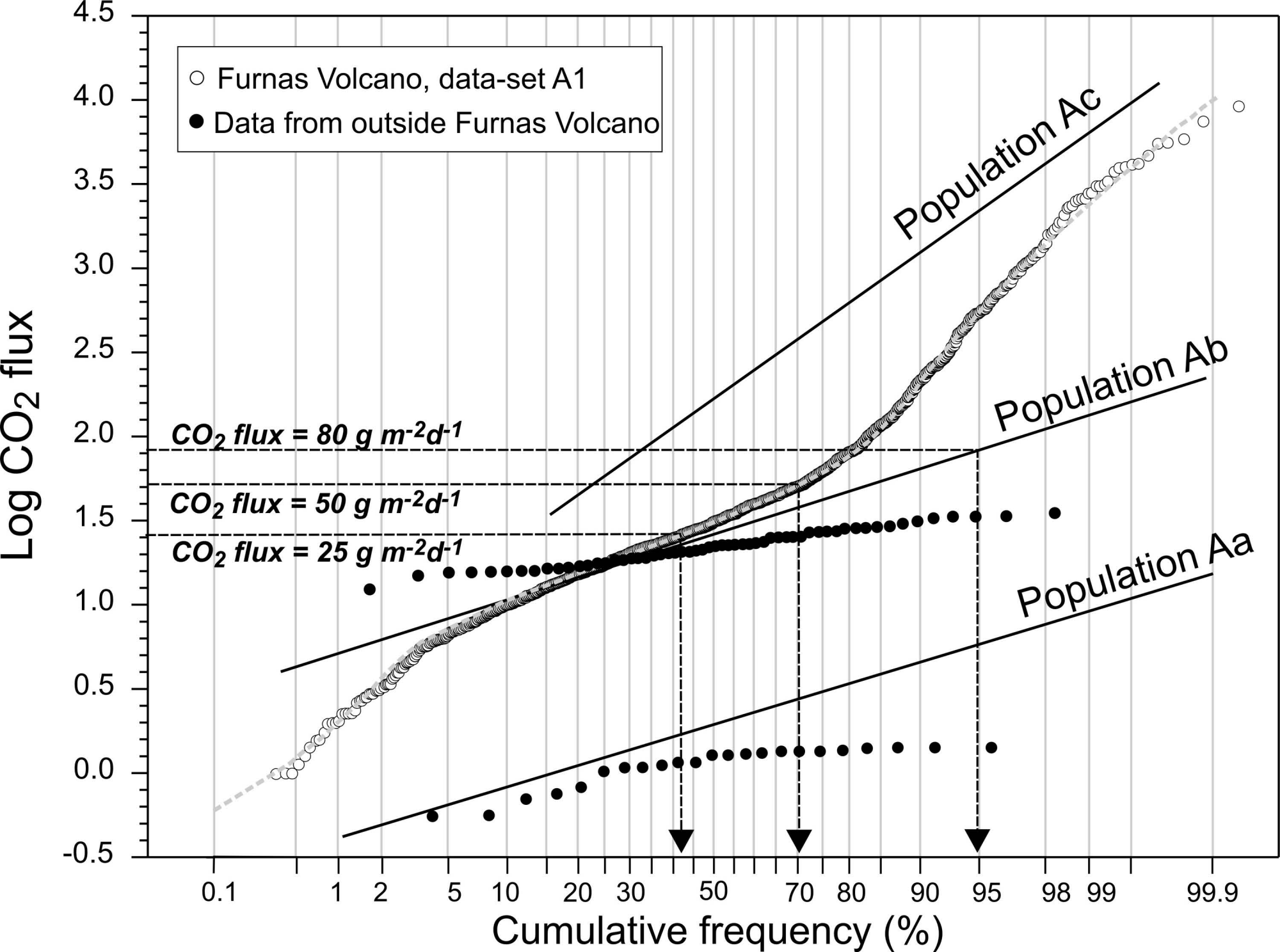
Furnas Volcano, data-set A1
Data from outside Furnas Volcano
Population Ac
Population Ab
Population Aa
CO2 flux = 80 g m-2d-1
CO2 flux = 50 g m-2d-1
CO2 flux = 25 g m-2d-1
Log CO2 flux
4.5
4.0
3.5
3.0
2.5
2.0
1.5
1.0
0.5
0.0
-0.5
0.1
1
2
5
10
20
30
50
70
80
90
95
98
99
99.9
Cumulative frequency (%)

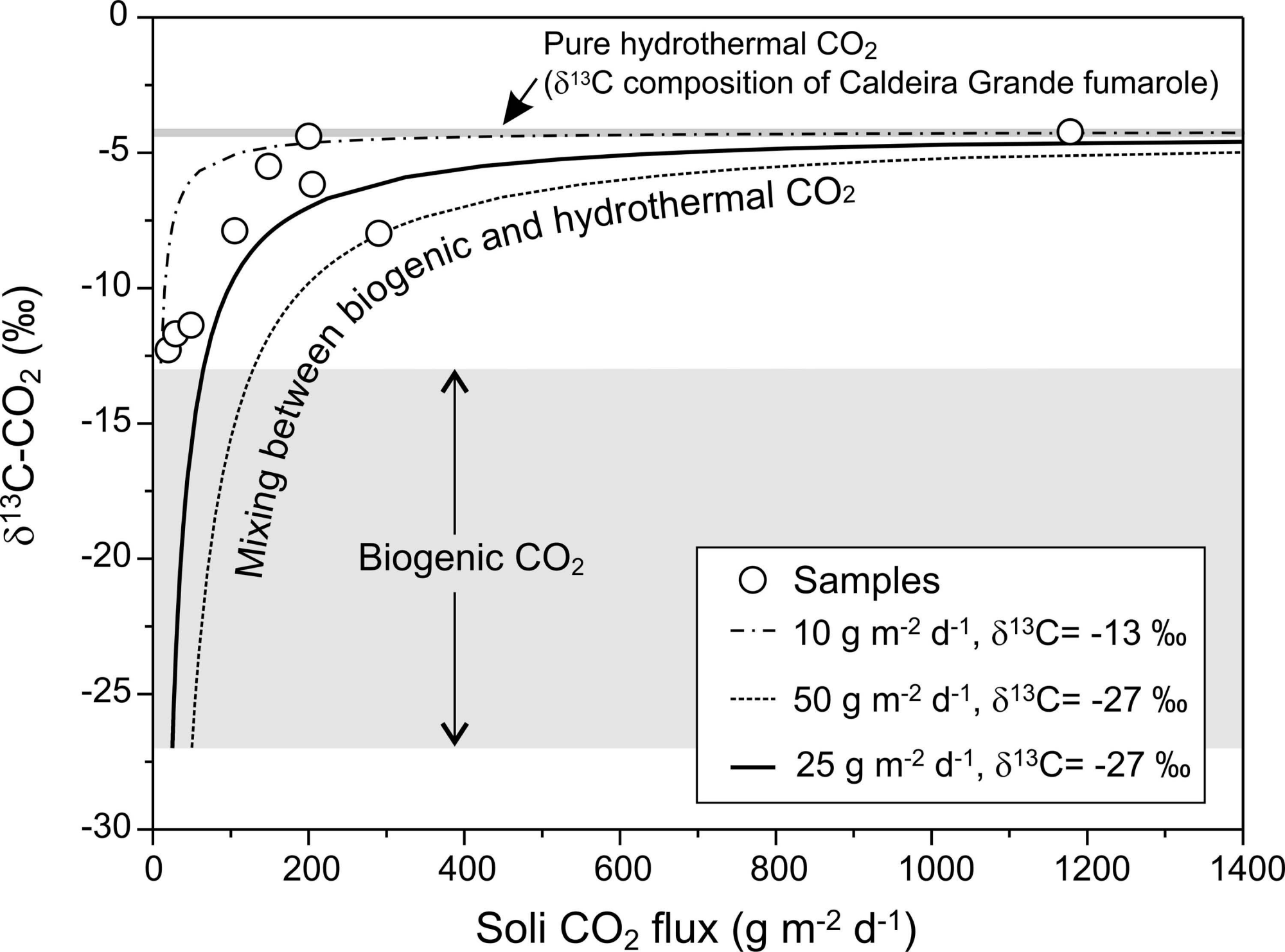
Pure hydrothermal CO_2
($\delta^{13}C$ composition of Caldeira Grande fumarole)
Mixing between biogenic and hydrothermal CO_2
Biogenic CO_2
Samples
10 g m^{-2} d^{-1}, $\delta^{13}C$= -13 ‰
50 g m^{-2} d^{-1}, $\delta^{13}C$= -27 ‰
25 g m^{-2} d^{-1}, $\delta^{13}C$= -27 ‰
$\delta^{13}C$-CO_2 (‰)
Soli CO_2 flux (g m^{-2} d^{-1})
0
-5
-10
-15
-20
-25
-30
0
200
400
600
800
1000
1200
1400

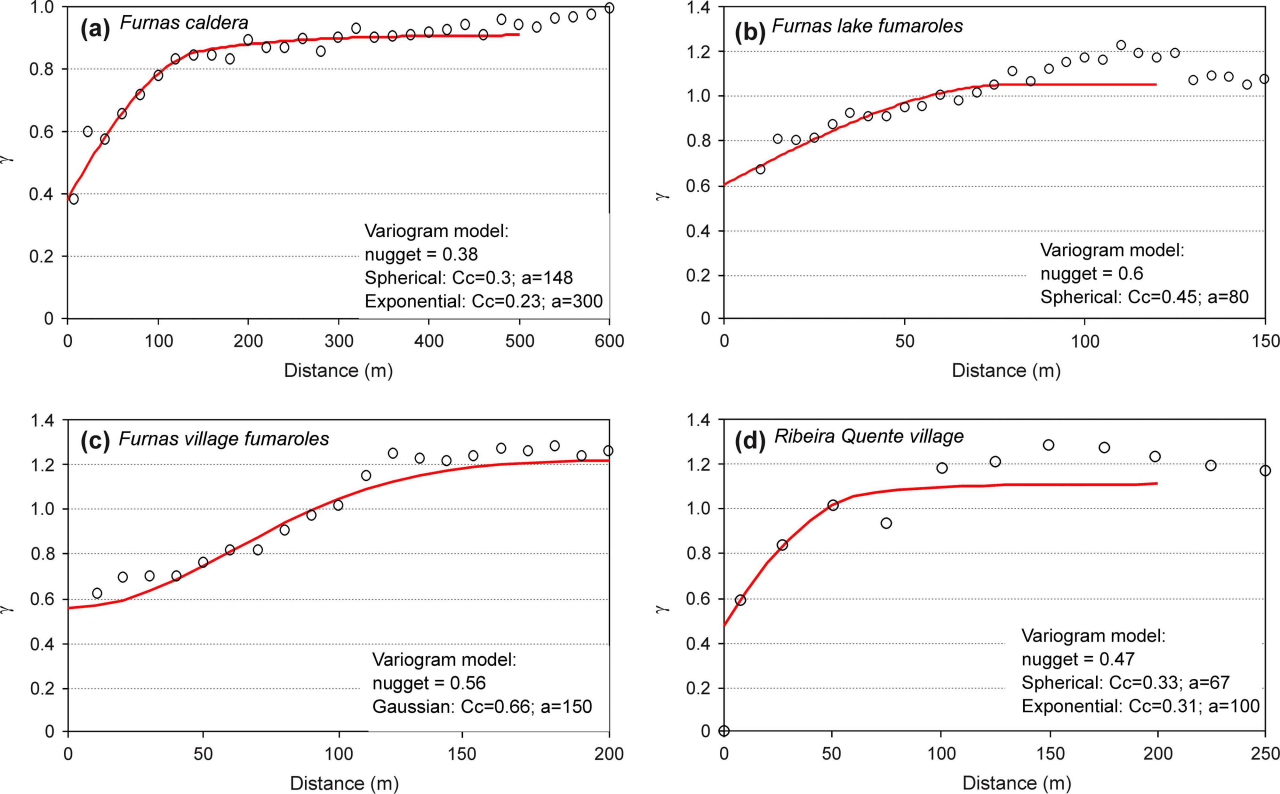
(a) Furnas caldera
γ
Distance (m)
Variogram model:
nugget = 0.38
Spherical: Cc=0.3; a=148
Exponential: Cc=0.23; a=300
(b) Furnas lake fumaroles
γ
Distance (m)
Variogram model:
nugget = 0.6
Spherical: Cc=0.45; a=80
(c) Furnas village fumaroles
γ
Distance (m)
Variogram model:
nugget = 0.56
Gaussian: Cc=0.66; a=150
(d) Ribeira Quente village
γ
Distance (m)
Variogram model:
nugget = 0.47
Spherical: Cc=0.33; a=67
Exponential: Cc=0.31; a=100

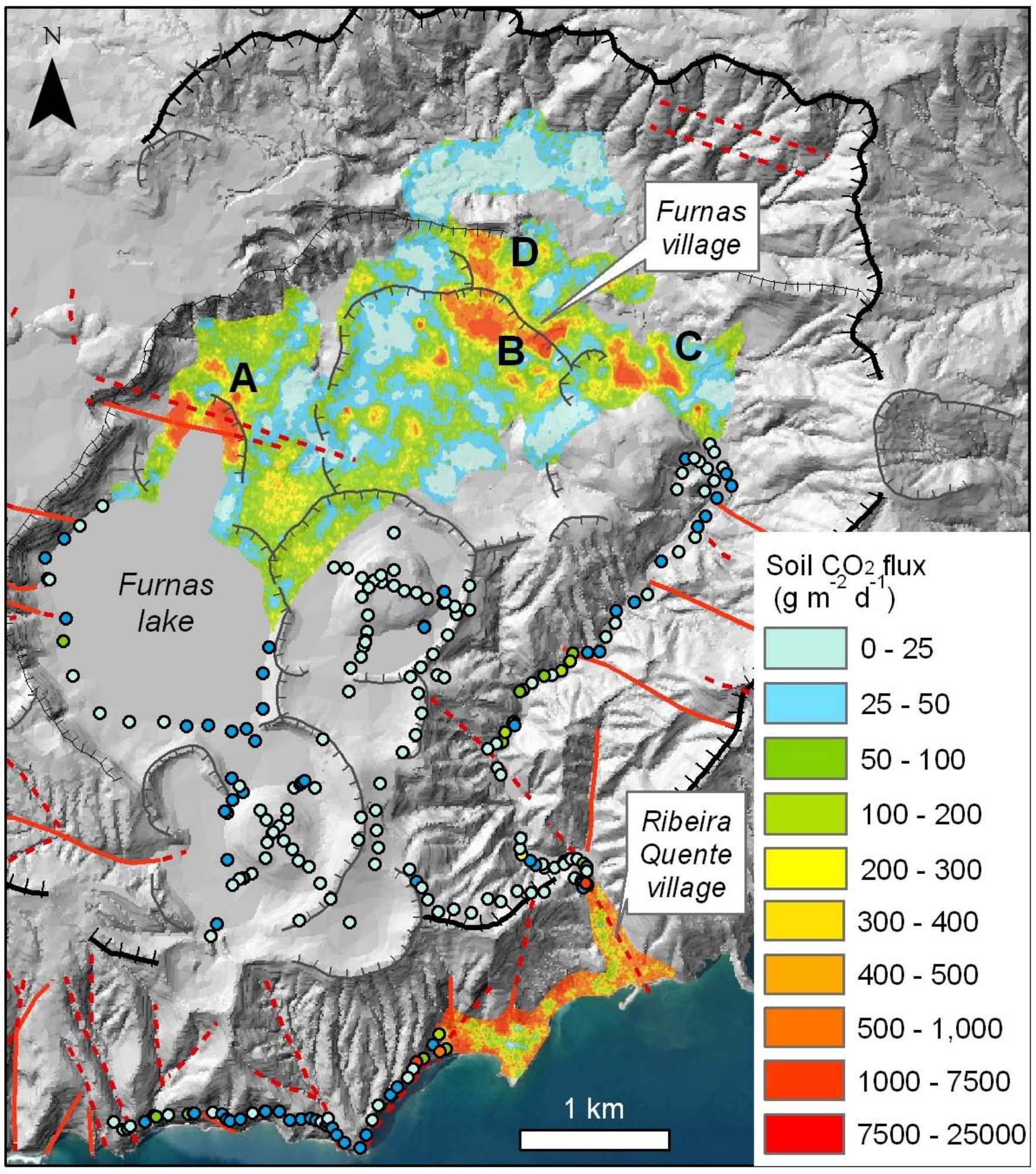
N
Furnas village
D
B
C
A
Furnas lake
Ribeira Quente village
1 km
Soil CO_2 flux ($g\ m^{-2}\ d^{-1}$)
0 - 25
25 - 50
50 - 100
100 - 200
200 - 300
300 - 400
400 - 500
500 - 1,000
1000 - 7500
7500 - 25000

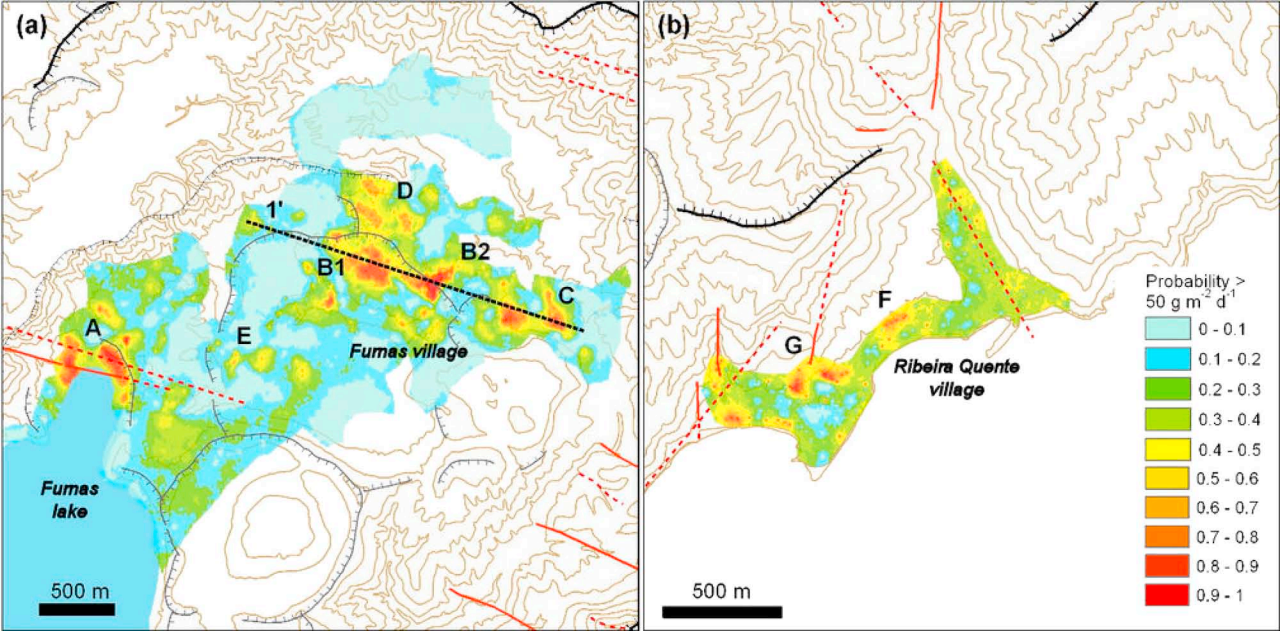
(a)
1'
D
B2
B1
C
A
E
Furnas village
Furnas lake
500 m
(b)
F
G
Ribeira Quente village
500 m
Probability > 50 g m-2 d-1
0 - 0.1
0.1 - 0.2
0.2 - 0.3
0.3 - 0.4
0.4 - 0.5
0.5 - 0.6
0.6 - 0.7
0.7 - 0.8
0.8 - 0.9
0.9 - 1

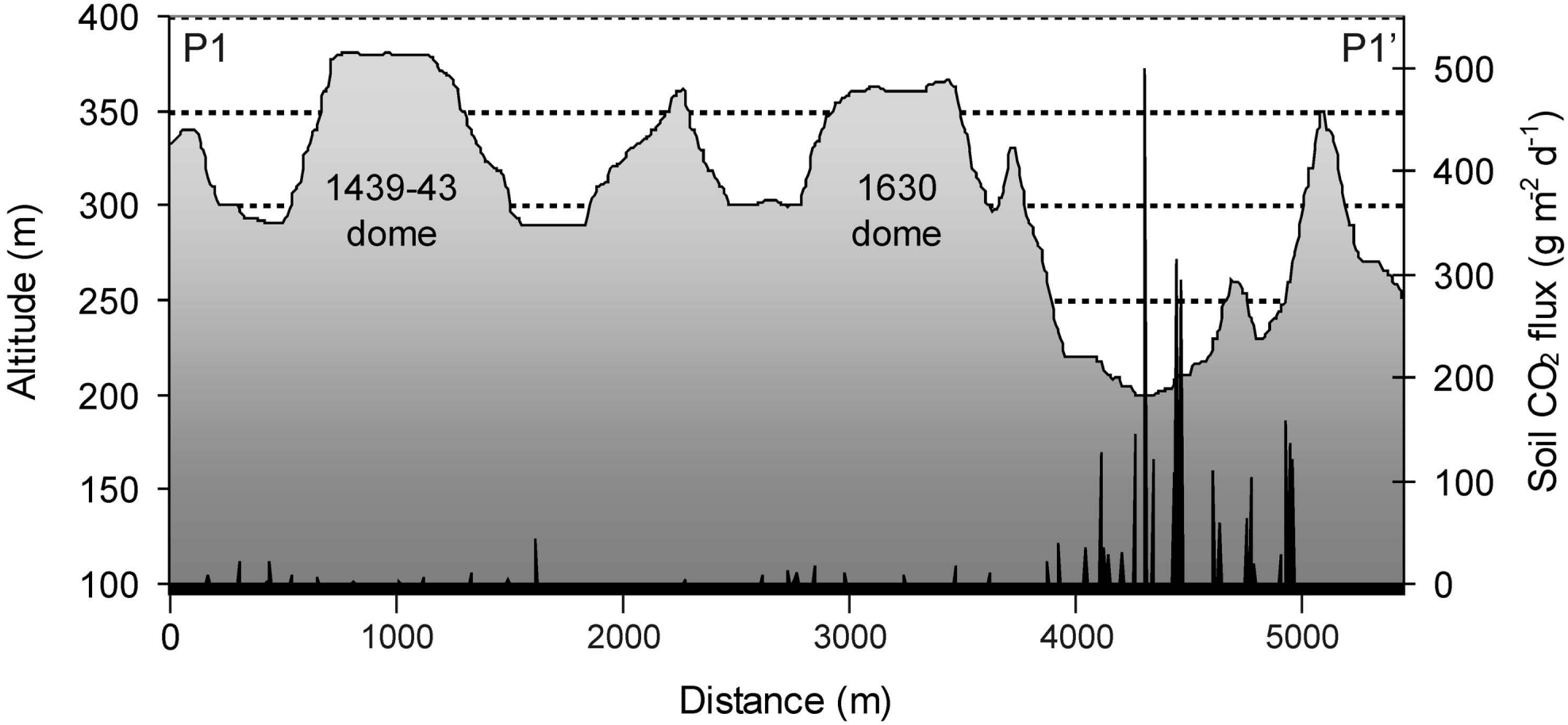
P1
P1'
1439-43
dome
1630
dome
Altitude (m)
Soil CO_2 flux (g m^{-2} d^{-1})
Distance (m)
400
350
300
250
200
150
100
500
400
300
200
100
0
0
1000
2000
3000
4000
5000

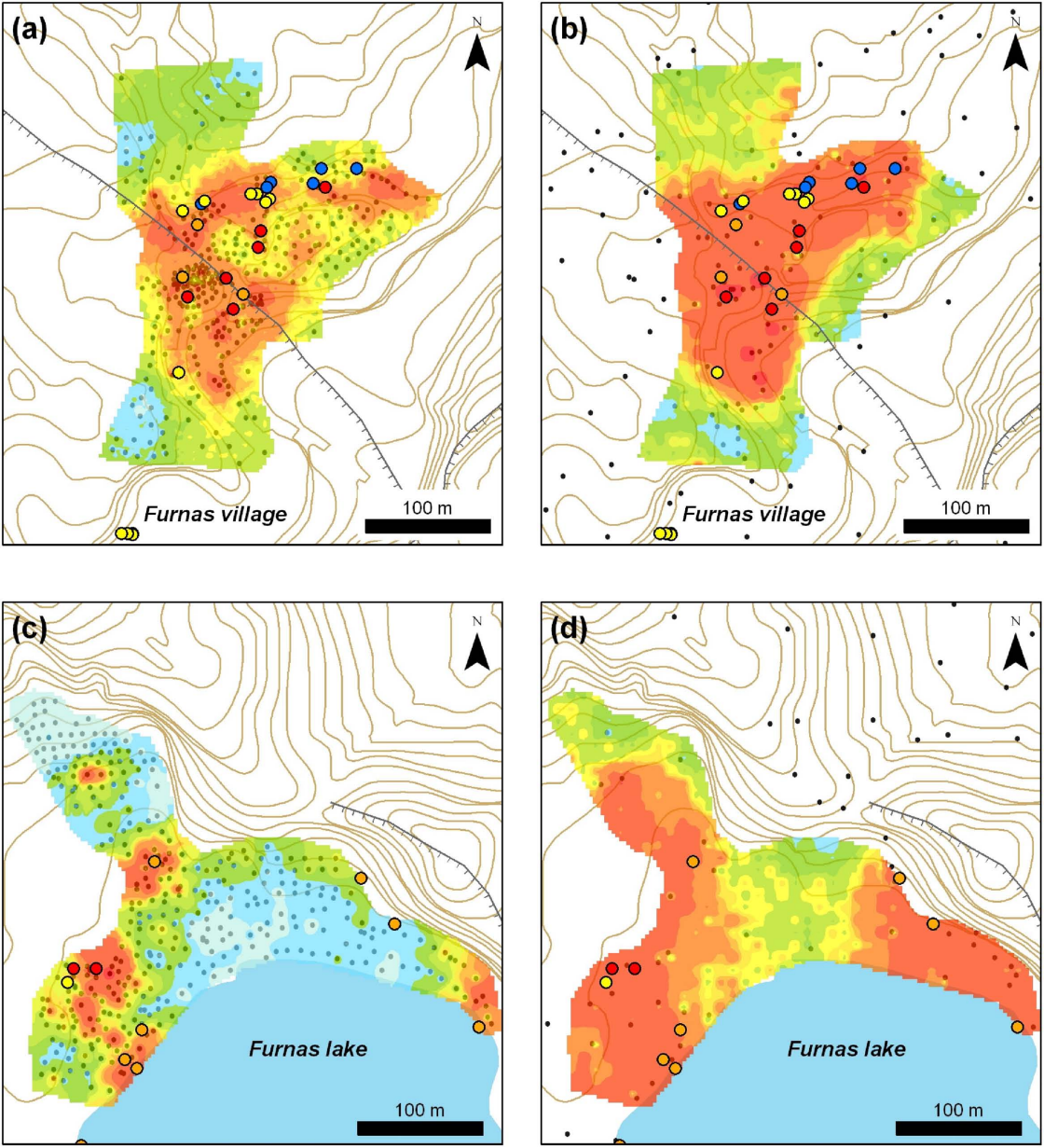
(a)
N
Furnas village
100 m
(b)
N
Furnas village
100 m
(c)
N
Furnas lake
100 m
(d)
N
Furnas lake
100 m